Chapter 8

Analysis of Color Images

The major objective of the color image analysis is to identify surface stains and other small defects such as small worm holes or small pin knots that are hard to detect in either the laser image or the X-ray image. However, the analysis of the color image is fully capable of detecting and identifying any of the visible defects that have been mentioned throughout the course of the discussion in the last two chapters. That is to say the system is capable of identifying all these defects in the form that they would present themselves at this stage of the processing, i.e., after the analysis of the laser image, $L(i, j)$, and the analysis of the X-ray image, $X(i, j)$, have both been completed. The complete list of defects that the analysis of the color image must be able to handle include surface stain, small or shallow mineral streak, small or shallow knots, small holes, wane containing bark, and small splits, i.e., special versions of all the defects that system is supposed to be able to identify. Note that all of these defects manifest themselves as a discoloration of the board's surface and hence are detectable in the color image.

The color image of a board's face is obtained using a color line-scan camera. The line-scan camera provides raw color image, $C_{RAW}(i, j)$, that has higher cross board spatial resolution than the raw images provided by either of the other two imaging modalities, i.e., $L_{RAW}(i, j)$ and $X_{RAW}(i, j)$, used on the system, i.e., 2.52 pixels/mm (or 64 pixels/inch) versus 1.26 pixels/mm (or 32 pixels/inch). Consequently, it provides the most detailed imagery of the board. Small defects such as split/cracks, worm holes, and pin knots are often visible in the color image while they are not visible in the laser, $L(i, j)$, or in the X-ray image, $X(i, j)$.

Of all the imaging modalities that have been discussed, the analysis of the color image involves the most preprocessing operations. One of these operations is shade correction. Shade correction is applied to the color image, $C_{RAW}(i, j)$, to remove the effects of both non-uniform lighting across the line that is imaged and any sensitivity differences that might exist in the image collection areas across the color line-scan camera's linear array.

To reduce the processing time needed for analyzing a color image while maintaining the ability to detect small defects, the cross board spatial resolution of the color image is reduced by a crack-preserving filter. The filter not only preserves the presence of small cracks in the reduced resolution image, $C_U(i, j)$, but other small defects as well. This is the second preprocessing operation that is performed on the color image. Note that $C_U(i, j)$ is unregistered color image that has been shade corrected and had it resolution reduced by the crack-preserving filter.

To significantly reduce the computational complexity of the analysis, the image segmentation operation and most subsequent operations are performed on the black and white image, $BW(i, j)$, that can be thought of as being created from the color image, $C(i, j)$, i.e., the registered color image that has been shade corrected and had it resolution reduced by the crack-preserving filter. The motivation for doing most of the analysis on $BW(i, j)$ will be given below. Remember that this black and white image, $BW(i, j)$, is perfectly registered to the color image, $C(i, j)$.

Other preprocessing operations that are performed on the color image include those described in Chapter 4 and 5.

Note, that most these preprocessing operations, with the exception of those that are described in Chapter 5, are performed by the MORRPH board [DRA95] and/or the associated data collection software. After this preprocessing has been completed the result is a color image, $C(i, j)$, and a black and white image, $BW(i, j)$. Note that $C(i, j)$ and the black and white image $BW(i, j)$ have 1.26 pixels/mm (or 32 pixels/inch) cross board resolutions and 0.63 pixels/mm (or 16 pixels/inch) down board resolution, i.e., the same spatial resolution as $L(i, j)$ and $X(i, j)$ have. It is these two images that are processed by the algorithms described in this chapter.

As to why a large portion of the analysis is based on $BW(i, j)$, a great deal of experimentation has shown that most surface defects (with the exception of some knots) can be accurately segmented using black and white imagery. In this work, the majority of knots have already been identified before the analysis of the color image is begun. This identification is

accomplished during the processing of the X-ray image, $X(i, j)$. Consequently, segmenting the black and white image, $BW(i, j)$, to locate potential defect areas does not compromise the ability of the system to detect the defects that remain after the analysis of both the laser and X-ray images have been completed.

However, color information is sometimes needed to identify certain defects. In these cases, component measures for gauging color information are extracted from components in the color image, $C(i, j)$, that correspond to the components in $BW(i, j)$. Computing these measures is easily done because $C(i, j)$ and $BW(i, j)$ are perfectly registered.

The analysis of color image is similar to that of the X-ray image and contains four processing levels: image preprocessing, low-level processing, intermediate-level processing and high-level processing. While most of the preprocessing is done by the MORRPH board and/or the data collection software which are not part of this research, the algorithms used will be described anyway so that the readers will understand the extent of all the processing that is done. The low-level processing includes image segmentation and connected component labeling. In the intermediate-level processing, initial measurements are extracted from the components formed by the connected component labeling process. Small components are subsequently eliminated and components that are very similar and close together are merged with a component merging operation. And finally, additional more complicated measurements are extracted from the remaining components. Note that just as was the case in the processing of the X-ray image, the analysis of the color image may require that additional measures be computed from the laser image, $L(i, j)$, and/or the X-ray image, $X(i, j)$.

The high-level processing of the color image attempts to assign a defect label to each of the components that remain after small component elimination and component merger has been performed. The high-level processing has access to all the information that is available in any of the other two imaging modalities. Hence, this high-level processing is capable of labeling any possible defect area that has been detected during the low-level processing. Finally, this high-level processing is also responsible for labeling any of the components that could not be

identified during the analysis of the laser image. To label these components, the system may, once again, compute additional measures from the color, black and white, or X-ray images.

This chapter describes the algorithms used in analysis of the color image and demonstrates some of the processing results that have been obtained using these algorithms.

Finally, just as was the case in Chapters 6 and 7, the low-level vision algorithms described in this chapter are only applied to color pixels or black and white pixels that are from the board's surface. This is possible because of the processing that was described in Chapter 5. This processing computes the values for *Board_Start*, *Board_End*, and *Board_Edge*. The algorithm for using *Board_Start*, *Board_End*, and *Board_Edge* to find pixels that only come from the board's surface is straightforward and will not be described below.

8.1 The Preprocessing of the Color Image

In general, image preprocessing is used to reduce the noise in an image that is caused by the imaging device [GON92] and/or to compensate for some other limits of the imaging hardware [SAW77]. The analysis of the raw color image, $C_{RAW}(i, j)$, i.e., the color image that comes directly from the color line scan camera, requires that five preprocessing operations be performed. These operations are: 1) shade correction, 2) crack-preserving filtering, 3) averaging the color channels to create a black and white image, 4) image registration, and 5) foreground/background differentiation. Since image registration and foreground/background differentiation were discussed in Chapters 4 and 5, respectively, and since averaging the color channels to create a black and white image is straightforward, only the shade correction and crack-preserving filter operations will be discussed here.

These preprocessing operations whose input is initially the raw color image, $C_{RAW}(i, j)$, result in the creation of the color image, $C(i, j)$, and the black and white image, $BW(i, j)$. It is these images together with $L(i, j)$ and $X(i, j)$ that will be used in this analysis.

8.1.1 Shade Correction

The first preprocessing operation that is performed on the color image, $C_{RAW}(i, j)$, is image shade correction [SAW77]. Shade correction is needed in order to remove any non-uniformity in lighting and/or differences in the color sensing elements across the line-scan camera's linear array of detectors.

Since the development of the shading correction algorithm for black and white cameras was given in Section 7.1.1 of Chapter 7, this discussion will not be repeated here. All that needs to be said here is that the color image, $C_{RAW}(i, j)$, is treated like three different black and white images where each of its red, green, and blue channels is treated as a separate black and white image. As will be remembered to shade correct a black and white image requires that two sets of constants be collected and stored. These arrays of constants are $g_{black}(x)$ and $g_{white}(x)$. Since the color image corresponds to three separate black and white images, six sets of constant values must be used. Let $g_{black,red}(x)$, $g_{whilte,red}(x)$, $g_{black,green}(x)$, $g_{white,green}(x)$, $g_{black,blue}(x)$, and $g_{white,blue}(x)$ denote these values. The meaning of this notation should be straightforward. The $g_{black,red}(x)$, $g_{black,green}(x)$, and $g_{black,blue}(x)$ values are obtained by collecting frames from the color camera while the lens's cover is on the camera lens. In this application 256 individual frames are collected and averaged together to get the three different sets of constant data. As for $g_{white,red}(x)$, $g_{white,green}(x)$, and $g_{white,blue}(x)$, these values are obtained by scanning a target that has uniform reflectance over the visible spectrum and which is brighter than anything that will be imaged while performing this application. (See [CON97] for more information about shade correction on this machine vision system.)

The output of the shade correction algorithm is $C_{RAW,SC}(i, j)$.

8.1.2 Crack-Preserving Filtering

For many, if not most, wood products related applications, manufacturers require a vision system that is able to detect very small (perhaps a better word is fine) splits, checks, cants, or flinches in boards so that these defects will not appear in the rough parts. Most small

splits/checks appear rather prominently in high-resolution black and white or color images of a board's surface. They show up as pixels that are darker, i.e., lower in intensity, than clear wood. Hence, for applications requiring color information, as this vision system does, a very high-resolution color camera must be used. Consequently, a large mount of data needs to be processed in real-time. This can markedly affect the speed at which the analysis computer must operate in order to perform the analysis in real-time. To reduce the required volume of data while maintaining the ability to detect small checks, a crack preserving filter was developed and incorporated into this vision system. It is implemented on the MORRPH board. It is applied to the color image, $C_{RAW,SC}(i, j)$ to yield the unregistered color image, $C_U(i, j)$. It is the output of this operation that becomes the color image input for the operations described in Chapter 4 and the unregistered black and white image, $BW_U(i, j)$, created by averaging the color channels of $C_U(i, j)$ that is the black and white image input for the operations described in Chapter 4.

In its most general form, the first step of the crack-preserving filter is to divide a color image into none-overlapping N×M color sub-images. The output of this filtering operation will replace each of these N×M color sub-images with a single color pixel, i.e., this color pixel will have the same color values as the pixel in the N×M sub-image that has the lowest intensity value. This is motivated by the fact that cracks are darker, lower in intensity, than clear wood.

More formally, The let the N×M color sub-image that is input to the filter be represented by three N×M arrays $R_{NM}(i, j)$, $G_{NM}(i, j)$ and $B_{NM}(i, j)$, which are red component, green component and blue component, respectively, of this sub-image. The output of the filter is a single color pixel whose intensity, $I_{NM} = [\, R_{NM}(i, j) + G_{NM}(i, j) + B_{NM}(i, j) \,]/3$, assumes its minimum value, i.e.,

$$I_{NM} = Min\left(\frac{1}{3}\left(R_{NM}(i, j) + G_{NM}(i, j) + B_{NM}(i, j)\right)\right), \; for\, all\; 0 \le i \le N-1, 0 \le j \le M-1 \qquad (8.1)$$

Obviously, the filter reduces the image size by a factor of NM, while preserving the presence of the dark pixels needed to detect small splits/checks.

This algorithm was implemented in software and tested on a number of samples to verify that it would indeed allow the detection of small checks in the reduced color image. For purposes of this study N = 1 and M = 2.

As was stated above, the output of the crack-preserving filter is unregistered color image, $C_U(i, j)$, an image that has the same resolution of the unregistered laser image $L_U(i, j)$ and the unregistered X-ray image $X_U(i, j)$. Note that $BW_U(i, j)$ is produced from $C_U(i, j)$ by simply averaging together the values of the color channels on a pixel by pixel basis. As such these two images are perfectly registered. All of these images are subsequently registered and stored as color image $C(i, j)$, the black and white image $BW(i, j)$, laser image $L(i, j)$, and X-ray image $X(i, j)$, respectively, as discussed in Chapter 5.

8.2 The Low-level Processing of the Color Image

As was stated in the introduction, the low-level processing of the color image, $C(i, j)$, involves image segmentation (remember the image to be segmented is the black and white image $BW(i, j)$) and connected component labeling. The segmentation algorithm that is used is based on finding dynamic thresholds on the histogram of the $BW(i, j)$. After this threshold has been selected then a new thresholded image, $BW_T(i, j)$, is created that is perfectly registered to the $BW(i, j)$. It is $BW_T(i, j)$ that is then input into the connect component labeling algorithm. The output of this algorithm is $BW_C(i, j)$. The creation of $BW_C(i, j)$ is the final step of the low-level processing.

As will be seen in the discussion given below, the low-level processing of the color image is very similar to the low-level processing of the X-ray image with many of the same algorithms being used. And, just as was the case in X-ray images, the effects of defects that have been previously identified in either the laser image processing or the X-ray image processing are removed from consideration before the low-level processing of the color image is begun. Theoretically, the removal of these defects should allow the histogram based thresholding segmentation procedure to be more sensitive in locating the presence of small defects. This removal is particularly important here since the thrust of the analysis of the color image is to locate small defects.

Before continuing, it is important to better defend the use of the black and white image, $BW(i, j)$, as the basis for all of the low-level processing. Color based segmentation methods are

more computationally complex than segmentation methods for black and white imagery [LUO93], and, consequently, segmenting color images requires considerably more time to complete than is required to segment black and white images. Therefore, one reason for using the black and white image, $BW(i, j)$, to do the segmentation is to reduce the computational complexity of this task.

This black and white image is perfectly registered to the color image. This black and white image, $BW(i, j)$, can be thought of as being obtained from the color image $C(i, j)$ using

$$BW(i, j) = \frac{1}{3}\big(R(i, j) + G(i, j) + B(i, j)\big)$$

where $R(i, j)$, $G(i, j)$, and $B(i, j)$ are the values of red, green, and blue components of the (i, j) pixel of the color image, C(i, j), respectively.

A great deal of experimentation has shown that most surface defects with the exception of some knots can be accurately segmented using black and white imagery [CON89, CHO91]. Moreover, as was indicated in the last chapter, X-ray image data together with information from color and laser images can be used to detect and identify knots accurately. The detection of knots using this information was all ready done in the analysis that of the X-ray image. Hence, the vast majority of knots have already been detected and identified before the analysis of the color image is even begun. As a consequence, the image segmentation that must be performed here can be based on the black and white image rather than on the color image $C(i, j)$ without any major reduction in segmentation accuracy. This is the second reason for using $BW(i, j)$ to do the segmentation.

Yet a third reason for using $BW(i, j)$ for doing the segmentation comes for studies conducted by Ohta [OHA80]. He has shown that (R + G + B)/3 is the most significant measure that one can use in color image segmentation. Based on these reasons together with experimentation that was performed during the course of this research suggests that $BW(i, j)$ is the right choice to use for the segmentation.

Note, however, that in the high-level processing of the color image where defect labels are being assigned, color information is sometimes needed to distinguish between certain kinds of defects such as small knots and mineral streaks. In such cases, component measures containing color information are extracted from the components in the color image $C(i, j)$ that correspond to the components of interest in the black and white image. This is easily accomplished since the black and white image is perfectly registered to the color image.

8.2.1 Removal of Defects Identified in the Laser and X-ray Image Processing

As was the case in the processing of the X-ray image (see Section 7.2.1), defects identified during the analysis of the laser image and/or the X-ray image are removed from consideration in the analysis of the color image. Unambiguous defects that can typically be identified during the analysis of the laser or the X-ray images include wane, thin board regions, knots, large mineral streaks, splits, and holes. The algorithm used to remove defects that have been identified earlier from the processing of the black and white image $BW(i, j)$ is the same algorithm that is used to remove defect areas from consideration in the analysis of the X-ray image.

While this algorithm is described in detail in Section 7.2.1, a brief review of this algorithm will be given here. More precisely, the purpose of this algorithm is to remove the effects defects identified in the laser and X-ray image processing from the histogram, H_{bw}, of the black and white image, $BW(i, j)$. To do this the histogram, H_{bwd}, of the defect regions on the board and the histogram, H_{bwb} of the whole board face are extracted from $BW(i, j)$. The histogram H_{bwd} is computed from all the pixels in every previously identified defect region, where each defect region includes a defect and the part of its surrounding area that is contained inside the minimum inscribing rectangle of that defect. The histogram, H_{bw}, with these defect areas removed, is computed using $H_{bw} = H_{bwb} - H_{bwd}$.

Next, just as was done in the X-ray image processing, for each pixel (i, j) within each defect region in the black and white image, $BW(i, j)$, the corresponding pixel in the thresholded black and white image, $BW_T(i, j)$, is assigned the value (-1). This is done before the connected-

component labeling operation is performed. In the thresholded black and white image $BW_T(i, j)$, the value 0 is used to represent background, any values greater than 0 are used to represent foreground objects. The value -1 is used to identify pixels in the removed regions.

Removing the defect components that have all ready been identified in either the analysis of the laser or the X-ray images increases the sensitivity of the thresholding procedure to small defects in black and white image. Therefore, more subtle defects in can be more easily segmented when the larger defect regions are removed.

8.2.2 Threshold Selection

The segmentation algorithm for segmenting the black and white image $BW(i, j)$ is almost exactly the same as the segmentation algorithm for segmenting the X-ray image. Both are based on the same basic assumptions, assumptions that are almost always true for this application. These assumptions are:

1. The total defect area on a board face is a small percentage (typically less that 10 percent) of the total area of the board's face.
2. Gray-level values of both clear wood and defects are normally distributed.

And as was discussed in Section 7.2.2, the first assumption follows from the quality of lumber used by typical secondary manufacturers. These manufacturers use boards whose surfaces are largely free of defects since less labor is required to saw up the rough parts when such boards are used as the raw input into the manufacturing operation. The second assumption is based on a good deal of experimental work that had been conducted over the past few years [CHO91].

A typical histogram, $H_{bw}(k)$, of a black and white image is shown in Figure 8.1. The very large peak, roughly between gray levels 90 and 150, is the clear wood peak. The values below gray level 90 show what the effects of small dark intensity, i.e., low intensity value, defects can have on this histogram. In this particular case it would be good if the threshold selection method could produce multiple thresholds between 0 and 90. For example, possible threshold values would be 20, 60 and 80, though these are only very approximate values. Also note that at the top of the clear wood peak there are two smaller peaks. These peaks are caused by slight intensity

differences between early wood/late wood. The threshold selection method must be able to cope with this double peak problem.

Since both of these assumptions are true for both the X-ray image, $X(i, j)$, and the black and white image, $BW(i, j)$, it is not surprising that the methods for finding thresholds in the histogram, $H_{bw}(k)$, of the $BW(i, j)$ should be about the same as finding thresholds in the histogram, $H_x(k)$, of the $X(i, j)$. Consequently, the argument that was given in Section 7.2.2 concerning the thresholding of X-ray images, applies equally well here. This means that what the thresholding operations must do is to find valleys and inflection points in the histogram data, whether the histogram be $H_{bw}(k)$ or $H_x(k)$. Not only this but both thresholding operations must be able to cope with double peaks that sometime occur in the clear wood portion of the histogram.

However, there is one major difference between these thresholding methods. In the X-ray image only two thresholds really count for anything. One of these is the threshold that separates clear wood areas from areas that are denser than clear wood. The other threshold is the one that separates clear wood areas from areas that are less dense than clear wood. However, in the segmentation of the black and white image, $BW(i, j)$, multiple thresholds on either side of the clear wood peak are desired thereby allowing such defects as surface stains, knot, split, mineral strike and holes (except through holes) all of which are typically darker than clear wood to be differentiated from one another.

Even given this difference the basically same procedure can be used with the exclusion of only two processing steps. The algorithm given in Section 7.2.2 for thresholding the X-ray image basically looks for any valleys or inflection points that it can find. This is exactly what needs to be done when segmenting the black and white image. Then, however, to arrive at only two thresholds mentioned above it starts with gray level 0 and looks for the largest valley point or inflection point that is smaller than the clear wood peak. The threshold found is the one that separates clear wood areas from areas that are denser than clear wood. It performs basically the same operation this time starting with gray level 255 and looking for the smallest valley or inflection point that is larger than the clear wood peak. This value, whatever it is, becomes the threshold that separates clear wood areas from areas that are less dense.

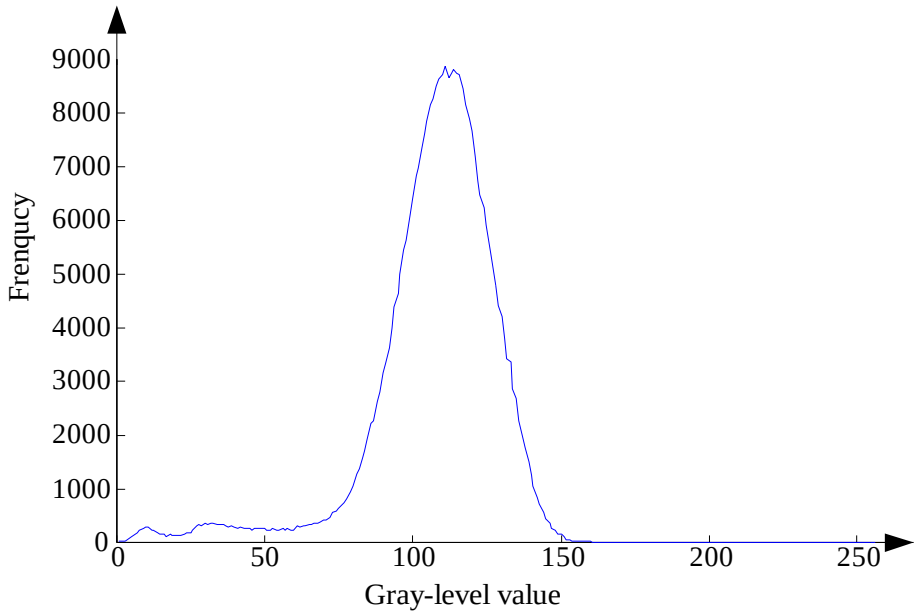

Figure 8.1 Typical histogram of the board part of the black and white image of a board surface

By eliminating these two search operations from the algorithm described in Section 7.2.2, all the valley points and inflection points are left in. This means that the segmentation of the black and white image should have more ability to differentiate defects that have only minor intensity differences from one another.

After the thresholds are found, intervals of the histogram between each two consecutive thresholds are assigned a unique interval label. All pixels that fall into an interval of the histogram are then assigned the value of the interval label as discussed in Section 7.2.2. The result of thresholding is stored in another image, the thresholded gray-level image $BW_T(i, j)$, which is registered to the gray-level image $BW(i, j)$.

8.2.3 Connected Component Region Labeling

Once pixels in the black and white image $BW(i, j)$ are segmented using the above thresholding operation to form $BW_T(i, j)$, the connected component labeling operation is subsequently applied to the thresholded image $BW_T(i, j)$. The goal of the operation is to form

initial components where each of these components might contain a defect. The connected component labeling algorithm described in Section 6.1.3 for finding the connected components in the laser image, $L(i, j)$, is used here to find the components in the color image processing.

The output of the connected component labeling operation is stored in a connected-component (or labeled) image $BW_C(i, j)$. The connected-component image typically contains several hundreds initial components, and each of these components is assigned a unique label. The image $BW_C(i, j)$ is used as input of intermediate-level processing that is discussed below.

8.3 Intermediate-level Processing of Color Images

The objectives of intermediate-level of processing are to extract measures from each of the components that were found in the connected component labeling operation, to eliminate small components, and to merge component that have similar properties. The measures that are extracted will be used later by the high-level processing to assign labels to the components, i.e., to determine to which defect class a component belongs. The possible defect classes are surface stains, knot, hole, and splits defect.

The intermediate-level processing that is performed on the black and white image is very similar to the intermediate-level processing that was performed on the X-ray image as should become apparent as the discussion proceeds.

8.3.1 Initial Measurement Extraction

The analysis of the color image requires that a number of measures be extracted. Since the color image, $C(i, j)$, and the black and white image, $BW(i, j)$, are perfectly registered, conceptually one should think of a component as having an existence in both the color image, i.e., having an existence in each of the three color channels, and having an existence in the black and white image as well. Given this situation all the components are defined in the image $BW_C(i, j)$. The initial measures that are extracted are as follows:

1) The area of the component is extracted from the image $BW_C(i, j)$.

2) The height and the width of the component's minimum inscribing rectangle is extracted from image $BW_C(i, j)$. Note the height is measured across board, i.e., a column measure, and the width is measured down board, i.e., a row measure.
3) The component's average gray level value is extracted from the black and white image $BW(i, j)$, and can be used to determine if a component is lighter or darker or of the same intensity as clear wood..
4) The component's average color, i.e., a three-dimensional vector whose elements are the average values of the red, the green and the blue channels over the component's extent, is extracted from the color image $C(i, j)$. This measure can be used to distinguish knots from mineral steak or stain.
5) The upper-left and lower-right corners of the minimum inscribing rectangle is extracted from image $BW_C(i, j)$. These measures also provide important information that can be used to quickly locate a component in $BW_C(i, j)$ or in any other image for that matter.
6) The touch_edge (total number of pixels that are on the perimeter of the component and touch the board's edge) is extracted from image $BW_C(i, j)$.

The above "initial" component measures are easy to compute and are extracted first. Of these measures two are needed immediately. These measures are used to do small component elimination and component merging. These measures are component area and component average gray level value. The other measures described above are extracted at this point of the processing because it is computationally efficient to do so.

In addition to above component measures, the largest connected component, i.e., the component that represents clear wood, is also identified here. Since it has been assumed that total areas of all the defects constitute only a small percentage of the total board area, the largest area should always be an area of clear wood. The average gray level value of this component is the average color intensity of clear wood and this value will be used to normalize intensity values of other components later. Similarly, the average values of the red, the green and the blue channels of the largest component represent the average values of the red, the green and the blue channels clear wood, respectively.

The output from this processing contains: 1) label of clear wood; 2) total number of components; 3) a list of components and an associated list of measures that were extracted from each of these components.

8.3.2 Small Component Elimination

As was discussed in Section 7.3.2, the initial components often contain many small (one or two pixel) meaningless components. These small components should be either eliminated if they are caused by noise or merged with similar adjacent components before further analysis is performed on the color image. The input to this operation includes: 1) the list of components and their corresponding measures extracted above; 2) the connected-component labeled image $BW_C(i, j)$.

The small component elimination used here is exactly same method discussed in Section 7.3.2. Details of this method can be found in Section 7.3.2.

The outputs of this operation, which is also the input of component-merging operation, consist of: 1) a new list of components, whose areas are larger than two, and their corresponding measures; 2) an updated image $BW_C(i, j)$, which no longer has any of the one- or two-pixel remaining in it.

8.3.3 Component Merging

Just as was the case in the analysis of the X-ray image, after the small components have been eliminated and merged there is still a need for doing more merging. And just as in the case with the X-ray image this merging involves the consideration of at least two statistical measures. Consequently, this merging must be based on a method that allows multiple statistical measures be considered in doing the merging operation. The method for handling the multiple measures is the same that was selected for use on the X-ray images and for the same reasons it is utilized here. The average transmission value of the X-ray image is replaced by the average gray-level

values of the black and white image. Details of the component-merging operation can be found in Section 7.3.3.

The combination of connected-component merging and small-component elimination has shown through experimentation to be effective at markedly reducing the number of components that must be considered by the high-level processing. This reduction has a very positive impact on the computation complexity of the high-level operations. Further, the experiments that have been connected indicate that this combination of operations does not adversely affect the defect labeling accuracy of this machine vision system

Finally, it should be noted that the connected-component merging and small-component elimination operations used here are based solely on information obtained from the black and white image. The reason for this is that it is computationally less complex to merge or eliminate regions based on black and white information than on color information. For example, using average gray level as a merging criterion requires one-third the computation as would be needed if the average color were used instead. Lastly, it should be pointed out that the merging results confirm the effectiveness of this operation without having to use color based information.

8.3.4 Additional Measurement Extraction

After the component elimination and merging operation are complete and the number of components that remain has been markedly reduced, more complex measures (as defined in Section 2.1) are then extracted from these remaining components. These more complex measures are extracted from either the black and white image $BW(i, j)$ or the color image $C(i, j)$. The more complex measures are as follows:

- For the component that has been identified as being clear wood the average values of the red, green and blue color channels for this component are extracted from the color image $C(i, j)$.
- The component's compactness defined as

$$CP = \frac{(perimeter)^2}{4p \cdot (area)}$$

is extracted from the image $BW_C(i, j)$.

- The component's elongatedness (as defined in Section 2.1) is extracted from the image $BW_C(i, j)$.

As will be seen in later in the description of the high-level processing yet more additional measures will have to be extracted. However, these additional measures are extracted from the X-ray image $X(i, j)$. These measures are extracted only when they are needed to accurately assign a label to a component. Note that these measures can be quickly computed since the black and white image and the X-ray image are nearly perfectly registered. Lastly note that this approach to measurement extraction saves processing time since measures are computed only when they are needed.

8.3.5 Intermediate-level Processing Outputs

The outputs of the intermediate-level of processing are: 1) A final version of connected-component image $BW_C(i, j)$ where each component has been assigned a unique label; 2) A list of components and their associated measures; 3) the total number of the final components found by intermediate-level of processing; and 4) the number or label of the component that represents clear wood. The outputs are then passed to the high-level processing of the color image.

The components together with their associated measures can be conveniently stored in an array whose elements are of a user-defined data type, e.g., a structure in C programming language. A structure is a collection of one or more variables, of possibly different types, grouped together to form user-defined data type. The structure used here to represent the components' measures is defined as:

```
struct component_measures
{     int   area,              /* Area measure of region     */
            perimeter,         /* Perimeter of the region    */
            ul_row,            /* Upper left row of MBR      */
            ul_column,         /* Upper left column of MBR*/
```

```
        lr_row,              /* Lower right row of MBR    */
        lr_column,           /* Lower right column of MBR*/
        component_label;     /* component label     */
    float avgray,      /* Average intensity of the component      */
        avg_r,         /* Average red level of the component      */
        avg_g,         /* Average green level of the component    */
        avg_b,         /* Average blue level of the component     */
        avg_trans,     /* average transmission value */
        hw_ratio,      /* ration of height vs. width */
        elongate,      /* Elongatedness measure of the component */
        compact,       /* Compactness measure of the component    */
        touch_edge,    /* Share boundary with frame / perimeter   */
        cm_row,        /* Row, center of mass for the component   */
        cm_column,     /* Column, center of mass for the component */
        contrast,      /* Local contrast measure of the r component */
        gray_var;      /* Gray level variance                     */
}
```

In this data structure `struct`, `int`, and `float` are key words in C programming language, and represent a user-defined date type structure, integer data type, and floating point data type, respectively.

Similar data structures are used in Chapter 6 and Chapter 7 to store the components and their associated measures. The variables (or members) in the structures used in Chapters 6 and 7 are slightly different from the structure used here. This is because the components in Chapter 6 and Chapter 7 have different associated measures.

8.4 The High-Level Processing of Color Images

Since the high-level processing of the color image is performed after the processing of the laser and X-ray images has all ready been completed, most of the large unambiguous defects

such as wane, mineral streak, knots, holes, and low/high density areas have all ready been identified by the system. Therefore, the major thrust of the color image analysis is to locate and identify the defects surface stain, shallow mineral streak, small holes, small knots, small wane and split/check. However, unlike the situation that existed in Chapter 7, the components that are analyzed by these defect recognition modules include components found in both the low-level processing of the color image, and components that have been detected in the analysis of laser images. The components that were found in the laser image and that will be considered here are those components that were assigned the *unknown* label during image segmentation. These components occur because the area of the surface of the board from which they come from is so dark that the reflected laser light does not have enough intensity to be detected by the laser imaging subsystem. This means that these components must be much darker than clear wood. The only defect classes for which this statement is true are surface stain, mineral streak, knot, wane, hole, and split. Since any large defect from one of these classes will be found and labeled during the analysis of the X-ray image, it is only the smaller instances of these defects that need be identified during the analysis of the color image, i.e., the classes that need to be considered to resolve components that could not be identified during the processing of the laser image are exactly the same classes as stated above. Given this fact, the high-level processing must only possess the capability of identifying the defect classes *surface stain*, *mineral streak*, *knot*, *wane*, *hole*, and *split*.

The high-level processing of the color image is implemented with several modules as illustrated in Figure 8.2. Each of these expert defect recognition modules is similar in function to those discussed in Chapter 7 for the high-level processing of the X-ray image. Just as in Chapter 7, each of these defect identification modules is designed to calculate a similarity measure, *approaching degree* (see Section 5.2), between components that it analyzes and the defect type it was designed to recognize.

The final decision is made based on the maximum value of the approaching degree. The component is assigned the defect class label for which the value of approaching degree is the largest and the value is greater than a threshold value (e.g., 0.4). If all values of approaching degree are smaller than the threshold, then the component is considered to be clear wood. All

these labeling results are then passed to a post-processing module that removes those defects that are inside another, and merges defects that have the same defect label and that are close to each other. Finally all defects identified are added to the final defect list.

After, all the components that were found in the analysis of the color image have been labeled, a second high-level processing operation is performed. This operation involves identifying the components from the laser image that result for the *unknown* label assignment during segmentation of the laser image. Note that since these components must be from the same defect classes as was considered in the above described analysis of the color image, the same defect recognition experts can be used to do this labeling operation. Since, the laser image provides virtually no information about what class each of these components might be from, this analysis of these components must only involve measures computed from the X-ray image and the color image. There is one last consideration that must go into the analysis of these components. Since they all must be dark in color it is highly probable that many of the defects they represent were all ready found and labeled in the previous analysis of the color image. However, it is also possible that some of components found in the laser image have not been found or labeled in the color image analysis. If this is the case then these components must be fed into the intermediate-level of processing so that the needed measures can be computed from their associated components in the X-ray and color image before high-level analysis of these components can begin.

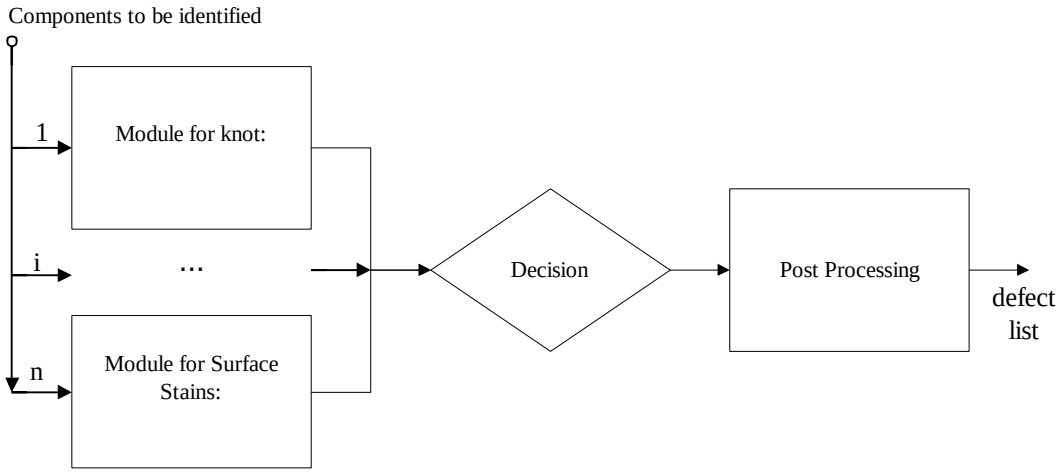

Figure 8.2 Architecture of high-level processing for color image

The algorithms for analyzing not only these components but also all the components will be described below. The description of the high-level processing will begin with a description of each defect recognition expert that must be used to do this high-level analysis.

8.4.1 Description of Expert Defect Recognition Modules

The expert defect recognition modules described below are applied to each component that is passed to the high-level processing. As will be seen, a number of these modules use the average transmission value, *d*, along with other measures to label the component that it is processing. Clearly, this average transmission value must be computed from the X-ray image, $X(i, j)$. However, since the connected component labeled image, $BW_C(i, j)$, is nearly perfectly registered with $X(i, j)$, computing the average transmission value of a component detected in the processing of the color image is relatively straightforward.

It should be mentioned that while a number of the expert defect recognition modules require the average transmission value as input and that while this average transmission value was not computed during the intermediate-level processing, it is only computed once for each component considered by the high-level processing. To see how this is accomplished one need only examine the data structure that was presented in Section 8.3.5. An examination of this data structure indicates that it has a placeholder, avg_trans. That is used to store the average transmission value. When a defect recognition module is applied to a component, the module first examines this location in the data structure. If this location contains a zero, a routine is called that computes the average transmission value and stores it in this placeholder location. If the value of this location is not zero, the expert defect recognition module assumes that this nonzero value is the average transmission value. Hence only one calculation of this value is required.

8.4.1.1 Surface Stain

The s*urface stain* class includes any discoloration on the surface of the wood. Stains may be caused by chemical or fungal action or they may be caused by soil or grease. Surface stains

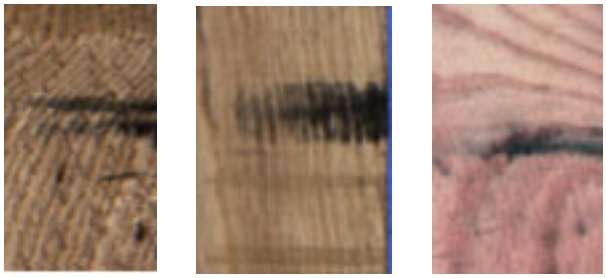

Figure 8.3 Typical surface stains

can virtually have any size or shape. In general, surface stains are dark in color and small in size. Some typical surface stains are shown in Figure 8.3.

A component that is an area of *surface stain* generally has the following characteristics:

- It appears as a dark area of any size in the black and white image. A typical shape for a surface stain area is a strip that is perpendicular to lumber grain.
- It has much lower red color channel intensity than clear wood has.

Surface stains generally are not visible in the X-ray image since they do not cause density variations in the wood where they appear. Therefore, a surface stain area in the X-ray should have the same density, i.e., transmission value, as clear wood. Surface stains generally are not visible in the laser image either since they do not cause any thickness variations in the board. For the darkest surface stains, i.e., ones that might reflect little laser light, the laser profiling system may not be able to sense these areas and, consequently, the thickness of these surface stains would be indeterminate.

Based on the above discussion about surface stains, a component that is a member of the *surface stain* class typically has the following characteristics:

1) The component's average transmission value, *d*, is approximately the same as clear wood. Any component that is not detected during the processing of the X-ray image should have an average transmission value that is very similar to that of clear wood. However, other defects such as surface knots can still have the average transmission values that are slightly greater than clear wood.

Hence, checking on this measure can help make a more accurate decision. The beginning of Section 8.4.1 explains how this measure is extracted.

2) The component's height/width ratio, *h*, is small since the component is usually a strip that is perpendicular to board grain. This measure can be computed from the height and width of the minimum inscribing rectangle. These measures were computed during the initial measurement extraction.
3) The component's average color intensity is usually low (darker) than clear wood. This property is measured by the component's normalized average color intensity. This measure is used in the analysis of the X-ray (see Section 7.3.3). It is defined to be the ratio of local average intensity to the average intensity of clear wood. The local average intensity is the average intensity of the component. The average intensity of clear wood is estimated by using the location of the largest peak in the histogram of the black/white image as the value for this measure. If two such peaks exist, the average value or the middle point of the two locations is used. Note that this measure can be computed from the average gray level value of the component, a measure extracted during the initial measure extraction, and the average color of clear wood, three values that are computed during the additional measure extraction processing.
4) The component is less red than clear wood. This feature is measured by the intensity normalized red value, *inr*. This measure was also used in the analysis of the X-ray image (see Section 7.3.3). It is defined to be the ratio of the average red channel value of the component to the average color intensity of the component. The local red channel value is the average red channel response of the component in the color image. The average local intensity value is the average of all three of the component's color channels in the color image. Note this measure can be computed from the average gray level intensity, a measure computed during initial measurement extraction, and the average color value of the component, three values also computed during the initial measurement extraction.

5) The component's area, *a*, is usually small. Remember the area was computed during the initial measure extraction.

Therefore, the *surface stains* class can be described by a fuzzy class $A_{stains} = \{A_{stains,transmissions}, A_{stains,height/width}, A_{stains,color\_intensity}, A_{stains,intensity\_red}, A_{strains,small\_area}\}$ where $A_{stains,transmissions}$ is a fuzzy set that represents the average transmission value with membership function $\mu_{stains,transmissions}(d)$, and $A_{stains,height/width}$ represents the small height/width ratio with membership function $\mu_{stains,\ height/width}(h)$. Fuzzy sets $A_{stains,\ color\_intensity}$, $A_{stains,intensity\_red}$, and $A_{strains,\ small\_area}$ characterize the other three component measures and have membership functions $\mu_{stains,color\_intensity}(ng)$, $\mu_{stains,intensity\_red}(inr)$, and $\mu_{stains,small\_area}(a)$ respectively. All these fuzzy sets are constructed in a manner that is exactly analogous to description that was given in Section 7.4.

For comparison purposes a component that is to be labeled is represented as the data sample $B = \{d_1, h_1, ng_1, inr_1, a_1\}$. The approaching degree between this component, i.e., data sample, and defect class *surface stains* is calculated using equation (7.15). The resulting computation becomes:

$$\begin{aligned} AD &= \sum_i w_i m_{A_{1i}} \\ &= w_1 m_{A_{11}} + w_2 m_{A_{12}} + w_3 m_{A_{13}} + w_4 m_{A_{14}} + w m_{A_{15}} \\ &= w_1 \mu_{stains,transmissions}(d_1) + w_2 \mu_{stains,height/width}(h_1) + w_3 \mu_{dstains,color\_intensity}(ng_1) \\ &\quad + w_4 \mu_{stains,\ intensity\_red}(inr_1) + w_5 \mu_{stains,\ small\_area}(a_1); \end{aligned} \qquad (8.2)$$

where the w_i's are weight factors and $\sum w_i = 1$. Here the weighting factors w_2 and w_3 are set to 0.3, the weighting factor w_4 is set to 0.2, and the weighting factors w_1 and w_5 are set to 0.1. The height/width ratio and the color intensity are considered to be more important than the other measures, consequently, their memberships are assigned larger weights. On the other hand the transmission value and component's area measures are considered to be less important, and, hence, both are assigned a small weight. These weight assignments are based on experiments that were conducted as part of this research activity. Currently, there is no theoretical guidance on how an optimal weighting assignment can be found.

8.4.1.2 Knots

The major reason that the *knot*s class needs to be reconsidered here is that there are some knots that are either very small or are shallow surface knots. In either case the density differences between these defects and clear wood are so small as to not be detectable in the X-ray image, $X(i, j)$. However, these knots typically can be detected in black and white image, $BW(i, j)$.

A component that is of one of these types, i.e., a component that is a member of the *knot* class, will have the following properties in either the black and white image or a color image;

- The component will have a small height/width ratio because these types of knots are typically circular or elliptical in shape. Note that this measure is easily computable based on the values of measures that were extracted during the initial measurement extraction operation.
- The component will have a high compactness. The component's compactness is computed during the initial measurement extraction step.
- The component is usually darker than surrounding wood. This property is measured by the component's normalized average color intensity. The definition of this measure can be found the previous section (Section 8.4.1).
- The component has a high red intensity when compared to the clear wood. This feature is measured by the intensity normalized red value, *inr*. This measure is defined in the previous section and can be computed from the set of measures extracted during the intermediate-level of processing.
- The component's average transmission value, *d*, is slightly greater than that of clear wood. See the beginning of Section 8.4.1 to see how this measure is extracted.

While small knots or shallow surface knots have density, i.e., transmission values in the X-ray image, that are approximately the same as that of clear wood, the average transmission value of a component that is one of these types of knots will still be slightly greater than clear wood. Hence, during the defect recognition phase this fact can be checked to help make a more accurate labeling.

Therefore, in a manner that is completely analogous to that described in Section 7.3.2, the *knot* class can be described by a fuzzy class $A_{knot} = \{A_{knot,transmissions}, A_{knot,height/width}, A_{knot,compactness}, A_{knot,color\_intensity}, A_{knot,intensity\_red}, \}$, where $A_{knot,transmissions}$ is a fuzzy set that represents the average transmission value with membership function $\mu_{knot,transmissions}(d)$, and $A_{knot,\ height/width}$ represents small height/width ratio with membership function $\mu_{knot,height/width}(h)$. The fuzzy sets $A_{knot,compactness}$, $A_{knot,color\_intensity}$, and $A_{knot,intensity\_red}$ characterize other three component measures and have membership functions $\mu_{stains,\ compactness}(cp)$ $\mu_{knot,color\_intensity}(ng)$, $\mu_{stains,intensity\_red}$ (inr), respectively. These fuzzy sets are constructed in an analogous manner as the ones in the previous section were.

The approaching degree between a data sample $\{d_1, h_1, cp_1, ng_1, inr_1\}$ and the defect class *knot* is given by the following equation:

$$\begin{aligned} AD &= \sum_i w_i \mu_{A_{2i}} \\ &= w_1\mu_{knot,\ transmissions}(d_1) + w_2\mu_{knot,\ height/width}(h_1) + w_3\mu_{knot,\ compactness}(cp_1) \\ &\quad + w_4\mu_{knot,\ color\_intensity}(ng_1) + w_5\mu_{knot,\ intensity\_red}(inr_1), \end{aligned} \tag{8.3}$$

where the w_i's are weight factors and $\sum w_i = 1$. Here the weighting factor w_1 is set to 0.1, the weighting factors w_2 and w_5 are set to 0.25 and the other weighting factors are set to 0.2. These weight assignments are based on experiments performed during the course of this research, i.e., these weighting values gave the best label assignment accuracy.

8.4.1.3 Wane

Wane is an area where the outer surface of the log is included in the board, i.e., part of the rectangular part of the board is missing because some of the rectangular parallelepiped that is the board is not there because it lies outside the exterior surface of the log. If bark is present in this wane area making this wane sound and square with the edge of the board, there may be no unambiguous indication of the presence of this wane in the laser image. As a consequence, this kind of wane is not reliably detectable in the laser image (see Figure 8.4). When bark is present in the way mentioned above, the wane area is usually small. Since the density of bark for most species of wood, in general, and for red oak, in particular, is not that different from clear wood it is also difficult to detect this wane in the X-ray image, i.e., there is little difference in

transmission value of bark and clear wood. The experiments that were conducted as part of this research all show that when such bark is present, the intensity of the wane area is significantly different from that of clear wood. Hence it is possible to detect the type of wane in the black and white image.

The experiments performed during this research suggest that a component that is a type of wane, i.e., part of the *wane* class, will generally has the following characteristics:

- The component is usually dark.
- The component is typically long and narrow where the long part of the wane is typically down the board and the narrow part is across the board. In general, the length of wane is at least several times greater than its width.
- The component typically varies in gray level across its spatial dimensions because the different anatomical parts of bark have different intensity values. Please note that for this type of wane the board on which it appears was cut in such a manner as to cut through the bark exposing more than one facet of the bark.
- The component is usually along an edge of the board since wane, by the way it is introduced into a board, generally appears on the edge of a board.

Given the above, a component of this type, i.e., one that is a member of the *wane* class, will have the following quantitative characteristics:

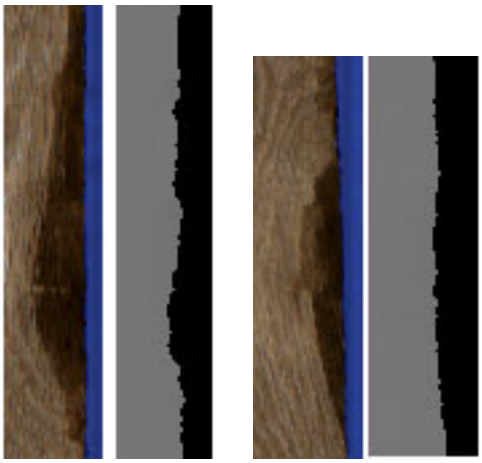

Figure 8.4 Wane in the color image (wane cannot be detected by laser/X-ray images)

1) The component's average transmission value, *d*, is the same as clear wood's. See the beginning of Section 8.4.1 to see how this measure is extracted.
2) The component's *touch_edge*, *te*, value is large. This measure is extracted during the initial measurement extraction operation.
3) The component's height/width ratio *h* is large. Note that this measure can be computed from values that were extracted during the initial measurement extraction operation.
4) The normalized average color intensity, *ng*, is low. This measure is defined in Section 8.4.1.1. Note that this measure can be computed from the average gray level value of the component, a measure extracted during the initial measure extraction, and the average color of clear wood, three values that were computed during the additional measure extract processing.
5) The component's local intensity variation, *lv*, is large. This measure is gauged by the variance of the intensity values for the pixels in the component.

Therefore, the defect class *wane* can be described by a fuzzy class $A_{wane} = \{A_{wane,transmissions}, A_{wane,touch\_edge}, A_{wane,height/width}, A_{wane,color\_intensity}, A_{wane,local\_variation}\}$. Fuzzy sets $A_{wane,transmissions}$, $A_{wane,touch\_edge}$, $A_{wane,height/width}$, $A_{wane,color\_intensity}$, $A_{wane,local\_variation}$ characterize the above five component measures and have membership functions $\mu_{wane,transmission}(d)$, $\mu_{wane,\ touch\_edge}(te)$, $\mu_{wane,height/width}(h)$, $\mu_{wane,\ color\_intensity}(ng)$, $\mu_{wane,\ local\_variation}(lv)$, respectively. All these fuzzy sets were constructed in a manner analogous to the way the ones in the previous section were.

A component forwarded by the lower level of processing can be considered as a singleton data sample $B = \{d_1, te_1, h_1, ng_1, lv_1\}$, the approaching degree of the data sample and defect class wane can be calculated by using equation (7.15):

$$\begin{aligned} AD &= \sum_i w_i m_{A_{3i}} \\ &= w_1 m_{A_{31}} + w_2 m_{A_{32}} + w_3 m_{A_{33}} + w_4 m_{A_{34}} + w m_{A_{35}} \\ &= w_1 \mu_{wane,\ normal\_density}(d_1) + w_2 \mu_{wane,\ near\_edge}(te_1) + w_3 \mu_{wane,\ height/width}(h_1) \\ &\quad + w_4\ \mu_{wane,\ color\_intensity}(ng_1) + w_4\ \mu_{wane,\ local\_var}(lv_1) \end{aligned} \qquad (8.4)$$

Where w_i's are weight factors and $\sum w_i = 1$. Here weight factor w_1 is set to 0.1, w_2/w_3 are set to 0.25, and others are set to 0.2. The transmission value is considered to be a less important measure than others, consequently, its membership weight is less than the others. In contrast, touch_edge and height/width ratio measures are considered to be more important, therefore, both are assigned a larger weight. These weight values were determined by experiments that were conducted during the course of this research, i.e., these weight values seemingly gave the best label assignment accuracy.

8.4.1.4 Small Holes

All large holes were detected and identified in the analysis of the X-ray image, $X(i, j)$. These large holes include large worm holes caused by loose knots that fell of the board, and other things. Clearly these holes are easily detected in X-ray image and since the analysis of the X-ray image labels everything that it detects these holes have already been labeled before the analysis of the color image was begun.

Experiments that were performed during this research have shown that it is not easy to detect small worm holes with X-ray images, especially, when such holes are not perpendicular to the lumber surface. The reason for this is quite simple, small holes do not result in much variation in transmission values from the transmission values of clear wood. To detect these small holes, the black and white image, $BW(i, j)$, must be used. Please remember that the original cross board spatial resolution of the color image was 2.52 pixels/mm (or 64 pixel/inch). This resolution was reduced the crack-preserving filter as discussed in Section 8.1. But, because of the nature of this filter, these small worm holes remain visible in the color image, $C(i, j)$. And, since the black and white image $BW(i, j)$ can be considered as being created from the $C(i, j)$, these holes are visible in $BW(i, j)$ as well. Finally, while the laser image and X-ray cannot be used to reliably detect small holes, these images will, depending on the quality of the nearly perfect registration with the black and white image, can provide information that is useful in identifying small holes.

A component containing a worm-hole or other small hole generally has the following characteristics in a black and white or a color image:

- Its ratio height/width is small. This is one of the major measures by which a small hole differs from a check.
- Its compactness measure is small due to its circular or elliptical shape.
- It is darker than clear wood.
- It contains less red component than normal wood.

Moreover, it may have some density variation (higher transmission value) when comparing with near-by wood. Therefore, its average transmission value can also be used to characterize the region.

Based on the above discussion, a component belonging to the class *hole* has the following characteristics:

1) The component's average transmission value (*d*) should be high. See the beginning of Section 8.4.1 to see how this measure is extracted.
2) The component's height/width ratio *h* should be low. This measure's value can be computed for values determined during the initial measurement extraction.
3) The component's compactness measure *cp* should be small. This measure was computed during the initial measurement extraction.
4) The component's normalized average color intensity value (*ng*) should be low. This measure was defined in Section 8.4.1.1 and as was noted there the value of this measure can be computed from measures that were evaluated during the measurement extraction operations.
5) The component's red normalized red value (*rnr*) should be low. The red normalized red value is a measure that was originally used in the analysis of the X-ray image, i.e., see Section 7.4.4. Its unusual name indicates that the average red value of clear wood is used to normalize the average red value of the component.

The fuzzy class, describing the *hole* class, $A_{hole} = \{A_{hole,transmission}, A_{hole,height/width}, A_{hole,compactness}, A_{hole,intensity}, A_{hole,red\_red}\}$ is constructed in a way that is similar to that discussed in Section 7.3.2. The fuzzy set $A_{hole,transmission}$ has a membership function called $m_{hole,transmission}(d)$, and the fuzzy set

$A_{hole,height/width}$ has a membership function called $\mu_{hole,height/width}(h)$, etc. All the membership functions are of the general form given in Equation (7.17). The parameters for each membership function are listed in Table 7.3.

The approaching degree between a data sample $B = \{d_1, h_1, cp_1, ng_1, nrn_1\}$, and class *knot* is determined by:

$$\begin{aligned} AD &= \sum_i w_i \mu_{A_{4i}} \\ &= w_1\mu_{hole,\ transmission}(d_1) + w_2\mu_{hole,height/width}(h_1) + w_3\mu_{hole,small\_compact}(cp_1) + w_4\mu_{hole,intesity}(ng_1) + \\ &\quad w_5\mu_{hole,red\_red}(rnr_1) \end{aligned} \tag{8.5}$$

where the w_i's are weight factors and $\sum w_i = 1$. Here weight factor w_1 is set to 0.1, w_2 and w_3 are set to 0.25, and others are set to 0.2. These weight assignments were determined by experiments performed during the course of this research, i.e., they seemingly gave the highest labeling accuracy.

8.4.1.5 Small Splits

Similar to small holes, small splits/checks are also hard to detect in X-ray images because these small defects cause very little variation of transmission value from that of clear wood. And similar as with small holes, splits/checks are typically very difficult if not impossible to detect in the laser image. Small splits/checks are typically 3 – 6 pixels in width. Though very small they are still detectable in the reduced resolution color image, $C(i, j)$, i.e., the crack preserving filter works very well at retaining their detectability in the reduced resolution color image. Since splits appear darker than clear wood in the color image, they are also detectable in the black and white image $BW(i, j)$. Given the above it should be clear that these defects will most likely be detected in the low-level processing of the color image. However as was the case in previous defect recognition modules, even though small splits/checks cause only minor variations in transmission value from that of clear wood, this minor difference can be used to help more accurately label them. But as will be remembered, the X-ray image and the color image are only *nearly perfectly* registered. Since splits/checks are usually very thin, the thinnest of the all the defect types, if this registration in not within a fairly tight tolerance, the information is extracted

from X-ray image may not really come from the region of the image where the split/check is actually located. In this eventuality the resulting information will not help in the labeling process.

A component that is a member of the split class, i.e., both splits and checks are put in this class, will generally appears as a component in the black and white or the color image with following characters:

- The component is darker than clear wood.
- The component usually is long and thin, i.e., long in the with grain (down board) direction and thin in the cross grain (cross board) direction.
- The component will be less compact than the other defect classes due to its long and narrow shape
- The component has a small width in relation to other defect types.

Given the above, a component belonging to the class *split* should have the following characteristics:

1) The component's average transmission value, *d*, should be slightly higher that clear wood's. Again, see the beginning of Section 8.4.1 to see how this measure is extracted.
2) The normalized average color intensity, *ng*, is low. This measure is defined in Section 8.3.1. Note that this measure can be computed from the average gray level value of the component, a measure extracted during the initial measure extraction, and the average color of clear wood, three values that were computed during the additional measure extract processing.
3) The component's height/width ratio *h* is large. Note that this measure can be computed from values that were extracted during the initial measurement extraction operation.
4) The component's compact measure, *cp*, should be large reflecting the fact that this component is less compact than those from other defect classes.
5) The component's width, *w*, is small.

The approaching degree between the class *split* and a given data sample is computed in the same manner as discussed above. The equation becomes

$$AD = \sum_i w_i m_{A_{5i}}$$

$$= w_1 m_{A_{51}} + w_2 m_{A_{52}} + w_3 m_{A_{53}} + w_4 m_{A_{54}} + w m_{A_{55}}$$

$$= w_1 \mu_{\text{spit, transmission}}(d_1) + w_2 \mu_{\text{split, height/width}}(h_1) + w_3 \mu_{\text{split, compactness}}(cp_1) + w_4 \mu_{\text{split,intensity}}(ng_1) + w_5 \mu_{\text{split, width}}(w_1); \quad (8.6)$$

where the w_i's are weight factors and $\sum w_i = 1$. Here $\mu_{\text{spit, transmission}}(d_1)$, $\mu_{\text{split, height/width}}(h_1)$, $\mu_{\text{split, compactness}}(cp_1)$, $\mu_{\text{split, intensity}}(ng_1)$ and $\mu_{\text{split, width}}(w_1)$ are membership functions of fuzzy sets $A_{split,transmission}$, $A_{split,height/width}$, $A_{split,compactness}$, $A_{split,intensity}$, and $A_{split,width}$ respectively. These fuzzy sets characterize the five component measures described above. All the fuzzy sets are constructed completely analogous to the way the fuzzy sets discussed previously were constructed. The w_i's are weight factors. All weight factors for the *split* class are currently all set to 0.2. These factors were based on experiments that were performed during the course of this research.

8.4.1.6 Mineral Streak

Similar to small knots, small/shallow mineral streak is often hard to detect in X-ray images. The reason for this difficulty is that small or shallow mineral streaks does not affect the transmission values very much and, hence, these transmission values are very close to that of clear wood. However, even small mineral streaks are often detectable in the reduced resolution color image, $C(i, j)$, i.e., the crack preserving filter works very well at preserving their detect-ability. Similar to splits/checks, mineral streaks appear darker than clear wood in the color image. Therefore, they are also detectable in the black and white image $BW(i, j)$.

A component that is from the *mineral streak* class will typically have the following characteristics:

- The component appears as a dark area with low gray-level values.
- The component's height/width ratio is usually high since mineral streak is often a long narrow strip that appears on the board face. It is typically long in the down board direction and narrow in the cross board direction.

- The component is usually less compact than the other defect types because it is usually like a long and narrow strip on the board face.
- It usually is less reddish than either clear wood or knots. The measure used to gauge this quality is called the intensity normalized red value, *inr*, as defined in Section 7.4.3.

Based on above observations, it would seem that a component that is from the *mineral streak* class can be described as follows:

1) The component's average transmission value, *d*, is very similar to clear wood though, perhaps, somewhat higher. See the beginning of Section 8.4.1 to see how d is computed.
2) The component's height/width ratio, *h*, is relatively high with respect to the other defect classes. As has been pointed out earlier, the height/width ratio can be computed from measures that are extracted during the intermediate-level of processing.
3) The component's compactness measure, *cp*, is relatively large reflecting the fact that this defect class is typically less compact than the other defect classes. This measure is computed during the intermediate-level of processing.
4) The component's normalized average color intensity (*ng*) is low. As stated before the normalized average color intensity can be computed from the measures extracted during the intermediate-level of processing.
5) The component's intensity normalized red value (*inr*) is low. The intensity normalized red value can be computed from the measures extracted during the intermediate-level of processing.

Therefore a fuzzy class describing *mineral streak* is given by $A_{\text{mineral}} = \{A_{mineral,transmissions}, A_{mineral,height/width}, A_{mineral,compactness}, A_{mineral,color\_intensity}, A_{\text{mineral,intensity\_red}}\}$ where the membership function for $A_{mineral,transmission}$ is denoted by $m_{mineral,transmission}(d)$, the membership function for $A_{mineral,height/width}$ is denoted by $m_{mineral,\text{height/width}}(h)$, the membership function for $A_{\text{mineral,compactness}}$ is denoted by $m_{mineral,\text{compactness}}(cp)$, etc. These fuzzy sets are constructed in a way that is similar to that discussed in Section 7.3.2.

For any given data sample, $B = \{d_1, h_1, cp_1, ng_1, irn_1\}$, the approaching degree of this data sample to the defect class *mineral streak* is given by:

$$AD_{mineral} = \sum_i w_i m_{A_{6i}} \quad (8.7)$$

$$= w_1 m_{A_{61}} + w_2 m_{A_{62}} + w_3 m_{A_{63}} + w_4 m_{A_{64}} + w m_{A_{65}}$$

$$= w_1 \mu_{mineral,\ transmission}(d_1) + w_2 \mu_{mineral,height/width}(h_1) + w_3 \mu_{mineral,\ compactness}(cp_1)$$

$$+ w_4 \mu_{mineral,color\_intensity}(ng_1) + w_5 \mu_{mineral,intensity\_red}(irn_1)$$

where w_i's are weight factors and $\sum_i w_i = 1$. As in the case of the *knot* class, all the *mineral steak* class weight factors are 0.2. That is to say each measure is given an equal weight.

8.4.2 Defect Identification and Post-processing

After a component, with its measures, has been processed by all these modules, the final defect type of the component is determined by a decision-making module. The module takes the values of approaching degree that were computed by the defect recognition modules for a component as its input. The decision-making module then selects maximum value of approaching degree for this component, and assigns the component a defect label based on the following criteria: 1) If this maximum approaching degree occurs say for defect class *K*, and if this maximum value is greater than a threshold value (e.g., 0.5), component is assigned the defect class label *K*. 2) Else if this maximum value is smaller than the threshold, then the component is considered to be clean wood, not a defect.

Once all components are identified, defects are subsequently fed into a post-processing module as discussed in Section 6.3.4. The defects that are overlapped or very closed to another defect will be merged. The distance between two defects is determined by distance between the minimum bounding rectangles (MBR) of the two defects as defined in Section 6.3.4. Once every defect region is processed, the resultant defect regions are added to the final defect list as mentioned in section 6.3.4.

8.4.3 Identification of the Components Marked as unknown During the Analysis of Laser Image

The components found in the laser image, but whose identity could not be determined based solely on the information from laser image (see Section 4.4.3), are stored in an array of a data structure and passed to the module described in this chapter that does the color image analysis. The data structure is similar to the data structure discussed in Section 8.3.5, but consists of different members:

```
struct components
{     int
            ul_row,             /* Upper left row of MIR       */
            ul_column,          /* Upper left column of MIR  */
            lr_row,             /* Lower right row of MIR     */
            lr_column,          /* Lower right column of MIR*/
            component_label;    /* Component label     */
            id_result;          /* identification result */          }.
```

where MIR stands from minimum inscribing rectangle. The final defect list, which contains defects identified in both the analysis of X-ray image and the analysis of color image, is also stored in another array of the same data structure.

For each component on the list of unknown components, a check is made to determine whether this component is overlapped with any defect on the final defect list. The component is considered to be overlapped with another defect, if the distance (defined by equation (6.3)) between the two minimum inscribing rectangle (MIR) of the two components is zero.

If component is overlapped with another known defect, it is usually not necessary to analyze this component since the component will be removed along with the identified defect. However, if the component is not overlapped with any defect, additional component measures must be extracted from the color image $C(i, j)$ and the X-ray image $X(i, j)$, and the component will be processed by above expert defect recognition modules in order to assign a label to this component. Effectively, these non-overlapping components are sent back to the intermediate-level processing for measurement extraction and the like.

8.5 Processing Examples

Two examples are presented here to strengthen the description of the algorithms that were given above and to illustrate how less than perfect early vision processing can still lead to a meaningful analysis of a board. Additional processing examples will be given in Chapter 9.

8.5.1 Removal of Defects Found Previously

As was discussed in section 8.1, defects were found during the analysis of the laser image and the X-ray should to be removed from all future consideration, in general, and from the processing of the color image, in particular. Doing so not only improves the quality of the segmentation of the gray-level image but also reduces the computation time as well.

The locations and extent of these defects in the black and white image (and/or the color image) are actually defined by minimum inscribing rectangles of the defects in the X-ray image or the laser image. Since the black/white image and the X-ray image (or the laser image) are "almost" perfectly registered just as the X-ray image and the color image are also "almost" perfectly registered. The same four steps discussed in section 7.1 are used to remove these defects from consideration. The pixels in these defect regions are marked with a special label -1 in the thresholded images, displayed as light colored rectangles in Figure 8.6. The value of -1 effectively differentiates these pixels from any foreground objects that are represented by values ≥ 1 and from background that is represented by a value of 0.

8.5.2 Image Thresholding and Connected Component Labeling

The segmentation is, in fact, performed on a black and white (or gray-level) image derived from a color image. The thresholds are dynamically determined with the algorithm discussed in section 8.1. Figure 8.5 illustrates the histograms of the black and white images extracted from the color images shown in Figure 8.6 (a) and (c). The background pixels are excluded from the histograms. In the histogram in Part (a) of Figure 8.5, the algorithm finds

three intervals. The precise range of each interval and the area of the board covered by pixels whose gray-level values lie in each interval are given in the Table 8.1.

And consequently, the thresholded image $BW_T(x, y)$ for image (a) in Figure 8.6 is given by:

$$BW_{T,a}(x,y) = \begin{cases} g_1 & if\ 0 \le BW(x,y) < 40 \\ g_2 & if\ 40 \le BW(x,y) < 64 \\ g_3 & if\ 64 \le BW(x,y) < 193 \end{cases} \tag{8.8}$$

where g_i is average gray level of *i*th interval. Obviously, the third interval [64 193) represents clear wood which occupies the majority area of the image.

For the histogram in Figure 8.5, Part (b), two intervals were found. The ranges of these intervals and the number of pixels contained in each are given in Table 8.1 (b). In this instance the second interval represents clear wood since this interval contains most of the pixels within the board image. Pixels falling into interval [1 72) are classified as one type, and pixels falling into interval [72 165) are categorized as clear wood. The thresholded image $BW_T(x, y)$ for image (b) in Figure 8.6 is, therefore, given by:

$$BW_{T,b}(x,y) = \begin{cases} g_1 & if\ 1 \le BW(x,y) < 72 \\ g_2 & if\ 72 \le BW(x,y) \le 165 \end{cases} \tag{8.9}$$

where g_i is average gray level of *i*th interval.

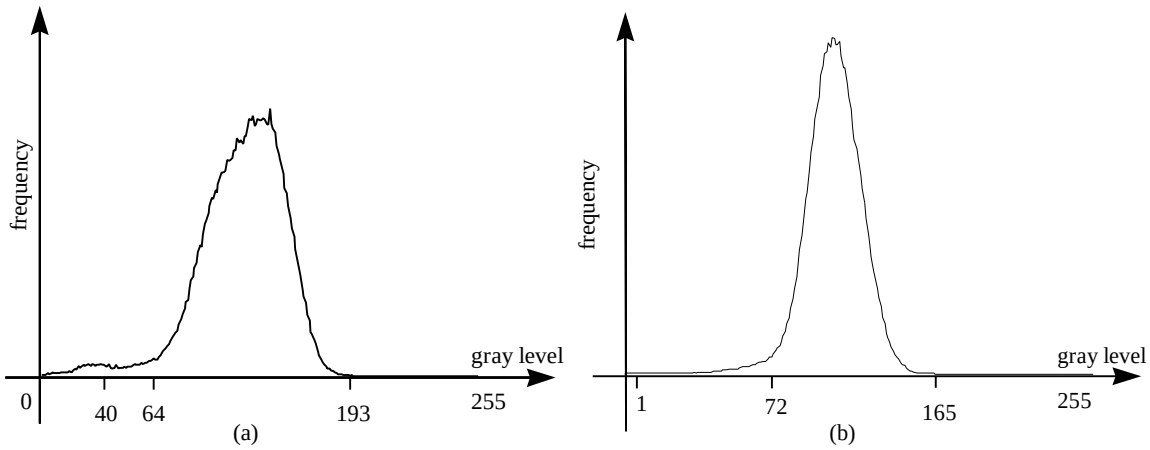

Figure 8.5 Histograms of two-gray level images

Table 8.1 Intervals found in the two histograms of Figure 8.5

(a)

Index	Intervals	Area
1	[0 40)	439
2	[40 64)	1685
3	[64 193]	216074

(b)

Index	Interval	Area
1	[1 72)	3621
2	[72 165]	299470

Figure 8.6 shows the original color images of the boards and their corresponding thresholded black and white images. The thresholded black and white image shown in Figure 8.6 (b) is created using Equation 8.8, while the thresholded black and white image shown in Figure 8.11 Part (d) was created using Equation (8.9). Clearly, pixels from the wane areas located at the lower part of the board shown in Figure 8.6 Part (a) are correctly separated from pixels that are believed to be clear wood. Pixels from the tiny wane areas in the middle part of the board shown in Figure 8.6 Part (a) are also separated from the clear wood. The light-colored rectangles represent the minimum inscribing rectangles of defects identified in previous analysis. For image (c) of Figure 8.6, pixels represent wane areas located at the upper part of the board are correctly separated from pixels that represent the clear wood. Pixels represent tiny knots and split located in the upper part of the board are also separated from the clear wood. Therefore, pixels from the major defect components (e.g., wane split, and knots) are separated from the clear wood in these gray-level images.

The connected component labeling is subsequently applied to the thresholded image to form the connected component image. Figure 8.7 (a) shows the connected component image that corresponds to the color image in Figure 8.6 (a). Here different connected components are displayed as various shades of pink. The pink shade used was determined by the value of the

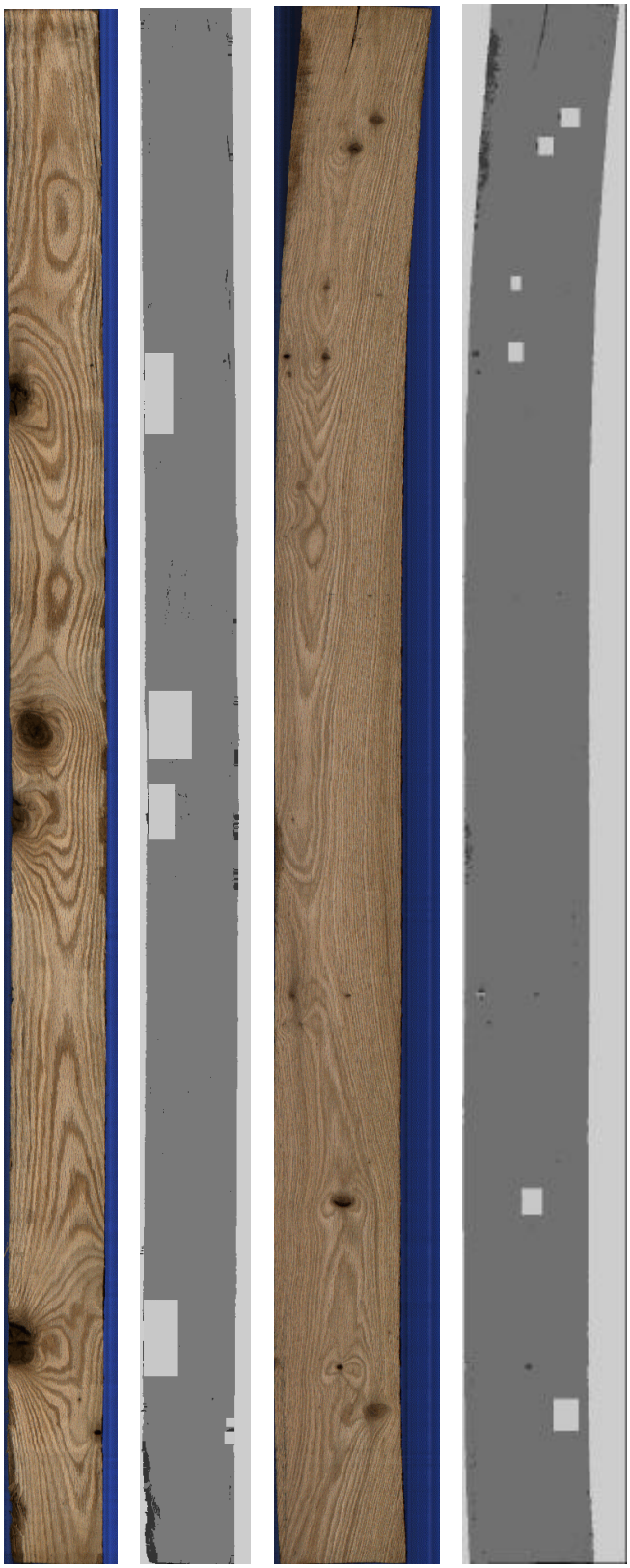

(a) (b) (c) (d)

Figure 8.6 Original color images and their thresholded gray-level images

label that was assigned to the connected component by the connected-component labeling operation. If the label assigned to the clear wood component, an assignment that is determined dynamically during connected-component labeling operation, is smaller than the labels of other components, then clear wood component will appear darker than other components when it is displayed. This is the case in Figure 8.7 (b), the connected component image that is corresponding to the color image in Figure 8.6 (c). Moreover, the clear wood of one board may appear to be darker than the clear wood of another board, if label values of clear wood components are different during the labeling process. See, for example, the clear wood components of Figure 8.7 (a) and (b). The minimum inscribing rectangles of defects identified previously are displayed as light green rectangles.

The output of low-level processing is a connected-component image, $BW_C(i, j)$, that contains components that possibly represent all or part of a potential defect. Pixels within each component are marked with a unique number – component label. The connected component labeled image is used as the input to the next level of processing – the intermediate-level of processing.

8.5.3 Measurement Extraction from the Black and White and the Color Images

From each component, a number of basic measures are extracted from the image $BW_C(i, j)$. These measures are then used to eliminate small components and to merge similar components. The measures are as follows:

- The area, a, of the component;
- The average intensity level, i, of the component;
- The upper left and lower right corners of the minimum inscribing rectangle of the component;
- The height and width of minimum inscribing rectangle of the component;
- The perimeter, i.e., the total number of pixels on the boundary, of the component;
- touch_edge, i.e., the total number of pixels on the boundary of the component that touch an edge of the board;

(a) (b)

Figure 8. 7 The connected component images of Figure 8.6 (b) and (d), before small component elimination and component merging

Subsequently, the small component elimination is applied to remove very small and meaningless components as discussed in Section 8.2. Then, a component merging operation is performed to merge similar adjacent components. Both of these operations use the measures defined above. The former operation eliminates components containing 1 or 2 pixels, and can reduce the total number of components that must be processed later by up to 70 percent. The component merging operation typically reduces the number of components that must be considered to less than 50 in most color images.

The effectiveness of both operations is illustrated in Table 8.2. The columns of this table represent the various sizes of components that are to be counted, i.e., one- or two- pixel components, components having pixel counts between 3 and 20 and, finally, components that have more than twenty pixels. The second row of this table gives the number of components by size that are in the connected-component labeled image of the board shown in Figure 8.6 Part (a), i.e., in the connected-component labeled image shown in Figure 8.7 Part (a). Similarly, Row 3 of this table provides the same information about the board shown in Figure 8.6 Part (c), i.e., the connected component labeled image of Figure 8.7 Part (b). In Row 2, the one- or two-pixel components account for 54 percent of total components, while in Row 3, 61 percent of the components contain one or two pixels. Removing these meaningless components will result in markedly reduced computational complexity. Table 8.3 has basically the same format as does Table 8.2. In rows two and three it shows that the number of 1 or 2 pixel components left after small component elimination. As can easily be observed all these small components have been eliminated. Table 8.4 shows the number of components that rename after the component merging operation is completed. As can easily be seen the total number of components that must be considered after the component merging operation is vary small in relation to the number of components that were originally found. In fact, the total number of components that remain in either image is less than 25 while the number of initial components found in each image numbered in several hundreds.

Table 8.2 Initial components found in the images of Figure 8.6

Component Size (in pixels)	1 or 2	3 – 20	> 20	Comments
Number of Components	113	77	19	Image (a)
Number of Components	186	97	24	Image (c)

Table 8.3 Components distribution after eliminate small components

Component Size (in pixels)	< 2	2 < 20	> 20	Comments
Number of Components	0	32	19	Image (a)
Number of Components	0	33	25	Image (c)

Table 8.4 Components distribution after component merging

Component Size (in pixels)	< 2	2 < 20	> 20	Comments
Number of Components	0	3	11	Image (a)
Number of Components	0	5	19	Image (c)

Figure 8.8 shows the connected component images of the board displayed in Figure 8.6 (a) and (c). As with Figure 8.7, the different connected components are displayed as various shades of pink. But the pink shade used was determined by the value of the label that was re-assigned during component merging operation. As one might see, the two images in Figure 8.8 contain many fewer small components comparing to the two images in Figure 8.7.

Even after component merging, there may still exist small components that contain only a few pixels, e.g., less than 20. Such small components are typically caused by noise, or small but real defects such as small worm holes or small knots. Therefore, these small components cannot be neglected. Similar to the small components in the analysis of the X-ray image, there are two options for handling these small components. These options are: 1) If defects are smaller than a threshold, e.g., 9 pixels in size, and can be neglected based on the manufacturer's specifications, then mark these small components as clear wood. For this case, the intermediate-level processing module applies an adjustable threshold to its final output. Any components with an area smaller than this threshold will be dropped from further consideration. 2) Process these small components as a regular component would be processed. The first option was selected for this system because most manufacturer's specifications allows for very small defects to appear in the finished product.

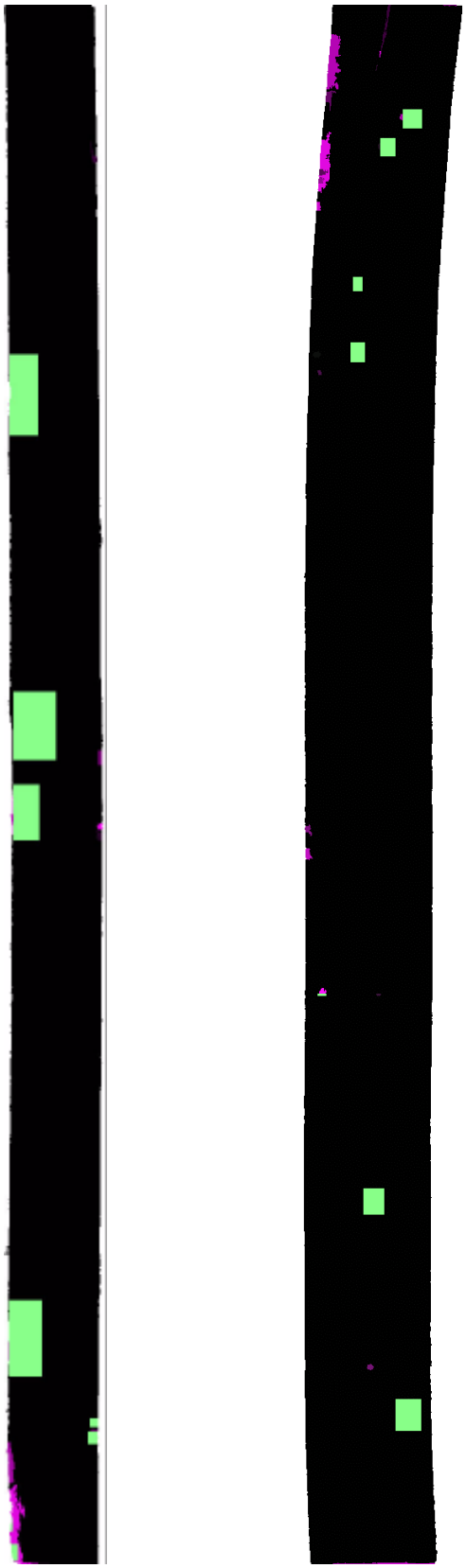

(a) (b)

Figure 8.8 Final results of intermediate-level of processing for images in Figure 8.6

After a component is merged with a similar component, component measures associated with the resultant component from the merging must be recomputed. That is, the area of the component, the height and width of its minimum inscribing rectangle, its average gray-level value, the upper left corner and lower right corned of its minimum inscribing rectangle, its perimeter, and its touch edge value must all be recomputed. Once component-merging operation is finished, a series of new measures are computed or extracted from each of the remaining components. These new measures are:

- variance of the gray-levels in the component
- compactness *cp* of the component
- elongatedness of the component
- average values of the red, green and blue components
- average transmission value extracted from the X-ray image

After these new measures have been computed from each of the remaining components, these components together with their associated measurement sets and the connected component image $BW_C(i, j)$ are used as inputs to the high-level processing module.

The low and intermediate-level processing modules have been applied to more than 300 images of red oak, maple, and pine boards. In almost all cases, the segmentation results detect the majority of defects such as knots, mineral streak, holes, and split/check that appeared in these boards. This suggest that the dynamic methods used to do the segmentation are, at least in part, species independent since they seem to work about equally well on all the species to which they have been applied.

8.5.4 Defect Identification and Post-processing

In the high-level processing module, each of the components forwarded to it by the intermediate-level processing module is sent to each of the expert defect recognition modules that have been created for this system. The expert defect recognition modules include ones for identifying members of the *knot* class, members of the *surface stain* class, members of the *mineral streak* class, members of the *hole* class, members of the *split* class, and members of the

wane class. For each component, each of the expert defect recognition modules returns an approaching degree as to how close the component resembles the defect class the module was created to identify.

The approaching degrees between each component and each defect class are given in Tables 8.5 for the board shown in Figure 8.6 Part (a). Each row gives the all the approaching degrees for one component. The columns of this table represent the approaching degree between defect class knot, mineral streak, high-density, split/check, hole and low-density for the component whose row is being examined. The maximum approaching degree is shown in bold face. The final result or decision is made by the decision-making module is based on the maximum approaching degree, as displayed in the last column of Table 8.5.

The above identification results are displayed in Figure 8.9 (a). The three small wane components are located in the middle part of the board and are marked with small blue rectangles. The two knots, marked with small red rectangles, are small knots near the bottom of the board, while the split is a misidentified component that is located at the lower left hand corner of the board. Note, defects displayed in Figure 8.9 (a) include defects that were detected and identified during the analysis of the laser image, i.e., the wane areas at the lower-left hand corner. Defects that were detected and identified during the analysis of the X-ray image are also displayed in Figure 8.9 (a). These defects are the four big knots marked by red rectangles.

Once all components are identified, the post-processing module checks each defect to determine if the defect is overlapped with any defects that are on the final defect list. For the defect identified above, only one defect, the split, is overlapped with anther defect (wane), therefore, so it is neglected. However, if a defect is overlapped with a high density or low density defect, the defect will still be added to the final defect list. Consequently, all defects except the split are the added to the final defect list.

Finally, components that were found but cannot be identified during the analysis of the laser image are processed. Each component on the unknown component list is checked against all defects on the final defect list to determine if there are any overlaps. Regarding the image

shown in Figure 8.6 (a), all three unknown components are overlapped with defects on the final list, which often happens. Therefore, these components are neglected and no further processing is required.

Similarly, for the color image in Figure 8.6 (c), 19 components are detected as listed in Table 8.4. Among them, 7 components are identified as small knots that are marked with red rectangle in Figure 8.9 (b), two components are identified as being splits and are marked with pink rectangles. The rest of the components are identified as being clear wood. The larger knots displayed in Figure 8.9 (b) are defects that were identified during the analysis of the X-ray image. The post-processing module will finally merge these small knots that are overlapped with large knots. There were no unknown components from the analysis of the laser image.

Table 8.5 Approaching degrees for the components found in image shown in Figure 8.6 Part (a)

Component	Knot	Mineral	Wane	Stains	Hole	Split/ Check	Final result
1	0.10	0.10	0.10	0.17	0.23	0.15	wood
2	0.19	0.12	0.10	0.10	0.10	0.10	wood
3	0.23	0.19	0.10	0.10	0.10	0.10	wood
4	0.23	0.21	**0.55**	0.10	0.10	0.10	wane
5	0.15	0.17	**0.48**	0.12	0.10	0.10	wane
7	0.26	0.34	**0.51**	0.10	0.10	0.10	wane
8	**0.46**	0.29	0.10	0.11	0.10	0.10	knot
9	**0.52**	0.33	0.10	0.12	0.10	0.10	knot
10	0.10	0.10	0.10	0.10	0.32	**0.52**	split

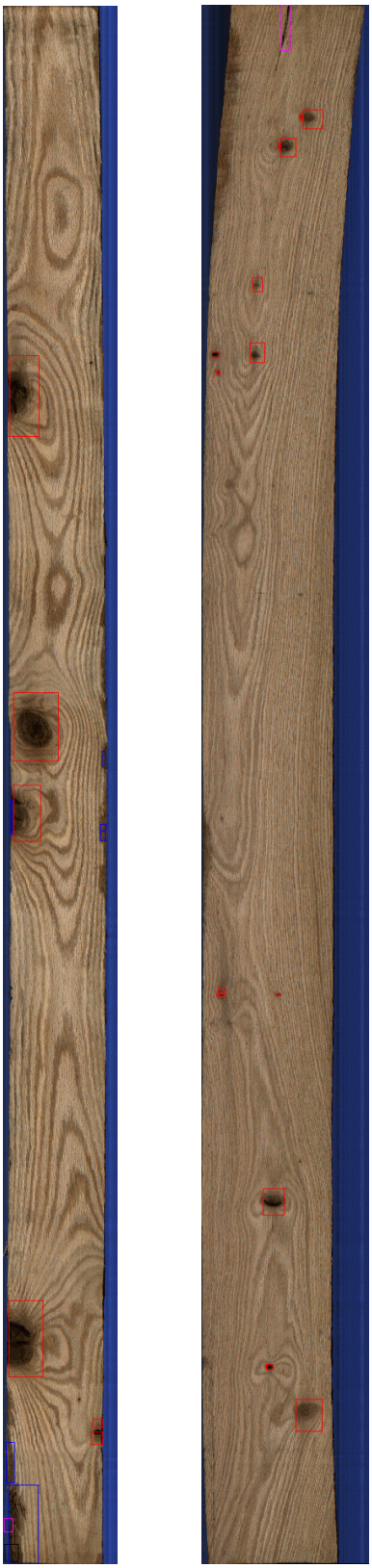

(a) (b)

Figure 8.9 Final results

8.6 Summary

The analysis of the color image is intended to detect surface stains and other smaller defects such as small knots, and small splits based on the variation of surface color together with information extracted from the X-ray image when necessary. The analysis consists of low-level processing, intermediate-level processing, and high-level processing that includes a post-identification processing operation. The goal of the low-level processing or segmentation is to find image components that might contain defects. The outputs of low-level processing module are then fed into intermediate-level processing module, where components that contain possible defects are found and measures that characterize each of these components are computed. In this intermediate-level processing small components are eliminated and similar components are merged. The final components and their associated measures are then sent to a high-level processing module, where each component is examined with additional measures extracted from the color image. If a component resembles a defect class, the component is then assigned the label of the defect class. The post-identification processing merges those components that are adjacent to each other and have the same defect label. Then all the components that have been assigned a defect label are put on a final defect list.

After this has been done, the high-level processing considers the unlabeled components that were found in the analysis of the laser image. It first examines all these components to determine which overlap a defect that is currently on the final defect list. Those components that do overlap are ignored since these components are part of what was all ready detected and identified during the processing of either the X-ray or the color images. For those components that do not overlap defects on the current defect list, measures are extracted from the X-ray and color images in an attempt to characterize them. After the measures have been extracted the same six defect recognition experts are applied to these components in an effort to classify them as being either of the knot class, the surface stain class, the mineral streak class, the wane class or the split class. Once these components have been labeled then the post-processing operation is applied to them just as it was with the components detected by the low-level processing of the color image.

The next chapter will present additional process results to demonstrate the capability of this vision system.

Chapter 9

System Performance

The purpose of this chapter is two folds. The most important objective is to demonstrate the capability and/or the overall performance of this vision system. This will be done in two ways. First, additional processing examples will be given. However, these processing examples in and of themselves provide only a glimpse of the system's capability. The only real gauge of system performance is to see how well it works with a particular application since some labeling errors may not adversely affect the output results of the application. This vision system was designed for the automatic crosscut application. Unfortunately, there has been no studies conducted to see how well the system works on this application. However, there has been a study, one that was conducted completely independently by other investigators, that addressed how well this vision system works in another application, the automatic grading of hardwood lumber. Therefore the results of this study will also be presented in this section. The second objective of this chapter is to illustrate how the various image analysis systems, the ones reported in Chapters 6 through 8, work together to locate and identify defects. This objective will be achieved by examining how the various defects were labeled as we consider the new processing examples.

In reporting the additional processing examples it should be noted that accurate defect labeling can only be achieved when all modules in the machine vision system (described in Chapters 4-8) work well in performing their respective tasks. That is, good recognition results can only occur if potential defect components are detected by the low-level processing algorithms, if the component measures extracted by the intermediate-level processing algorithms accurately characterize the defects, and if the labeling algorithms of the high-level processing can accurately label components based on these measures. Therefore, the first subsection of this chapter will focus on the final identification results obtained from lumber samples, samples that seemingly reflect those that would be processed or graded by the industry.

9.1 Example Results

Due to availability constraints of the image collection hardware, only a limited number (less than 100) of red oak boards were available for processing at the time this research was conducted. The red oak samples presented in this section were selected from the lumber images that were available. The boards, themselves, were kiln-dried to within 5 to 8 percent moisture content and were surfaced with an abrasive planer to create uniformly thick specimens and to remove any surface roughness, soil, and other such surface condition that could obscure wood defects. The board sizes varied in length from 1.8m (or 6 feet) to 3.7m (or 12 feet) and in width from 10cm (or 4 inches) to 30cm (or 12 inches).

This section will not only describe the processing results that were obtained from these boards but also indicate which of the various image processing systems, i.e., laser image processing, X-ray image processing, or color image processing, was responsible for locating and identifying each defect. The information that is passed from each of these modules to arrive at the final defect classification result is also discussed in this section.

The discussion will begin by giving some examples that illustrate how the outputs of the laser image processing module are used by the other processing modules and how these modules continue to add to the list of defects that are found and identified.

The first processing example to be considered is shown in Figure 9.1. The is a rather simple board that has a small area of wane on the bottom left-hand corner of the board as can be seen in Figure 9.1 (c). This small area of wane was located and identified in the processing of the laser image. It is marked by a blue (used to represent wane) rectangle at the bottom of the board. This is accomplished even though the wane is not clearly visible in the laser image (Figure 9.1 (a)). The blue rectangle appears to be much bigger than the defect component. This is because the small wane component is connected to the thin region that appears along the board's bottom edge. Since both the wane area and the thin edge region are connected they are grouped into one component, hence the large size for this blue rectangle. Please note that this thin edge region is an imaging artifact. This problem can be corrected if the last two lines of the

laser images are automatically pre-processed (e.g., assigned a range value of clear wood) or discarded by the image collecting software.

The board has two large knots and a high-density area. All three of these defects are clearly visible in the X-ray image (Figure 9.1 (b)). All three of these areas are located and identified in the processing of the X-ray image. The two knots are marked with red (representing knot) rectangles. Note that one of the knots, the one towards the top along the left edge, actually is marked by two red rectangles. Only the larger rectangle is due to the processing of the X-ray image. The high-density area is marked with a white (representing high-density) rectangle.

As will be remembered the analysis of the color image is primarily aimed at finding any small defects that remain after the analysis of the laser and the analysis of X-ray images have been performed. In the analysis of the color image a few small components of wane are found and identified. The components are all marked with the appropriate blue rectangles. These regions appear on both sides of the board. Also, as will be remembered, the defects found during the analysis of the other imaging modalities are removed from consideration during the analysis of the color image. When the knot that appears towards the top of the board on its left-hand side was found in the X-ray image, its full extent was not found during the low-level processing. Hence, when this knot area was removed from consideration in the color image a small, discolored area remained. This area was found and identified as a knot in the color image processing. It is marked by the small red rectangle that appears above the larger red rectangle that resulted from the processing of the X-ray image.

The second example that will be given (see Figure 9.2) also illustrates the analysis that is performed on laser image. Observe that the laser image (Figure 9.2 (a)) has a relatively low contrast that limits the level of thickness resolution. Also observe that there appears to be a seam in the middle of the laser image. This seam is the result of a slight misalignment between the two range cameras that are used to collect laser images (i.e., each camera can image up to 10.16 cm or 4 inches of board width). Currently, this misalignment is within 2 or 3 pixel values of each other. This does not cause a problem in the current laser image processing. Nevertheless, it is important to carefully consider the calibration of the imaging system to eliminate or minimize

(a) (b) (c)

Figure 9.1 A simple example that contains some wane and other defects.

(a) (b) (c)

Figure 9.2. The laser, X-ray and color images of a board that contains wane/thin board.

the effect of multiple cameras used to collect such board images as well as to minimize noise and vibration.

This example contains a large wane area on the top left-hand side of the board and a small wane area on the bottom right-hand side of the board. The wane area at the upper-left corner is clearly visible in the laser image (Figure 9.2 (a)). When the laser image was processed this wane area was broken into two separate components. The components were then correctly identified and this identification generated the two larger blue rectangles displayed in the color image shown in Figure 9.2 (c). However, between these two rectangular areas is an area of wane that has approximately the correct thickness and, hence, cannot be detected in the laser image. That is why this wane area was broken up into two components in the laser image processing. The other wane area is also clearly visible in the laser image. It, too, was correctly located and identified during the laser image processing. This identification generated the bottom blue rectangle. There are also several small areas of wane, located near upper-right edge of the board. These areas of wane all have approximately the correct thickness and, hence, are not easily detectable during the analysis of laser image.

Subsequently, the X-ray image is processed. The hole in the middle of the board is identified during the analysis of the X-ray image and is marked with an admittedly hard to see black rectangle (black represents hole). The hole is clearly visible in the X-ray image (Figure 9.2 (b)) but is not visible in the laser image (Figure 9.2 (a)). Two high-density areas were located and identified during the analysis of the X-ray image. They are marked with white rectangles. One of these is located about half way down the length of the board. The other, the smaller one, is located at the bottom of the board. The first high-density area, the one that surrounds the hole, is caused by high-density wood that typically occurs around some types of holes. The second high-density area, the one at the bottom of the board, has a density that is only slightly higher than clear wood. Hence, it is difficult to see this in the X-ray image.

During the analysis of the color image, the three wane areas on the upper right-hand side of the board are detected and correctly identified. A part of the wane area at the bottom of the board is also detected and correctly identified. This wane area generated the small blue rectangle

that is just above the larger one that was generated during the analysis of the laser image. Also, two small wane areas on the upper left-hand side of the board were also detected and correctly identified. These wane areas have almost the correct thickness and, hence, could not be detected during the analysis of the laser image. These two areas generated the two smaller blue rectangles shown. One of them lies between the two large blue rectangles. The other one is just below the lower of the two larger blue rectangles.

In the analysis of the color image two small areas were detected and incorrectly labeled as split. These two areas are marked by pink (representing split) rectangles. One of these areas is at the top of the board, almost adjacent to top most area of wane. The other is adjacent to the top area of wane that appears on the upper, right-hand side of the board. Obviously both were incorrectly labeled. This misidentification is the result of a remaining edge section that was not detected during the analysis of the laser image. Since the thickness of this edge section has almost the correct thickness, the full extent of wane was not captured during the analysis of the laser image. In the analysis of the color image these remaining edge sections have features that resemble splits. To address the problem of not finding the full extent of a defect in the analysis of the laser image, one could adjust the size of minimum inscribing rectangle of the defect to be increased by a user specified amount when removing the defect from consideration (see Section 8.1).

The big red rectangle near the bottom is a misidentified knot. The area was labeled a knot because the component's surface color is close to that of a knot and the component's average X-ray transmission value is slightly higher than that of the clear wood. This type of misidentification is a common error with single-sensor wood machine vision systems. While multi-sensor machine vision systems help provide additional information to avoid these errors, they can still occur as is demonstrated here.

There is one last thing that needs to be said about this last example. As will be remembered from the discussion in Chapter 8, when one defect lies completely inside another the final step is to remove the smaller defect from the final defect list. This is true from every class of defect except the high-density class. That is why it wasn't removed.

Before continuing with more examples, it is important to point out that the primary responsibility of the color image processing module is to find rather small defects since most of the larger defects have already been found and labeled in either the analysis of the laser image or the analysis of the X-ray image. The only exceptions to this are cases such as the mislabeled knot found in the last example.

The third example to be considered is a board that contains three large areas of wane, two at the top of the board and one at the bottom of the board, and a very interesting knot (see Figure 9.3). This knot is interesting because it is a so-called loose knot, one that contains a void. It is also interesting because this knot is surrounded by tension wood, i.e., a high-density wood that typically will not machine well and, hence, is considered a removable defect for the crosscutting application.

Because of the complicated nature of the knot area and surrounding tension wood, in this example the option to remove small defects lying inside larger defects was turned off so that the reader could see all the defect regions that were generated during the processing of all three imaging modalities.

During the analysis of laser image, two large areas of wane at the top and one area at the bottom part of the board were all located and correctly identified. This identification generated the large blue rectangles as shown in Figure 9.3 (c). These wane areas are clearly visible from the laser image in Figure 9.3 (a). There exist several small areas of wane, but these are not detected during the analysis of the laser image, since these wane areas have a similar thickness to the rest of the board. As will be seen, these areas are detected later during the analysis of the color image.

There is one last point that should be made about the laser image in Figure 9.3 (a). Note the very dark areas in the middle of the image. This corresponds to particularly dark areas of the color image. These areas of the board surface were so dark that the laser did not reflect enough

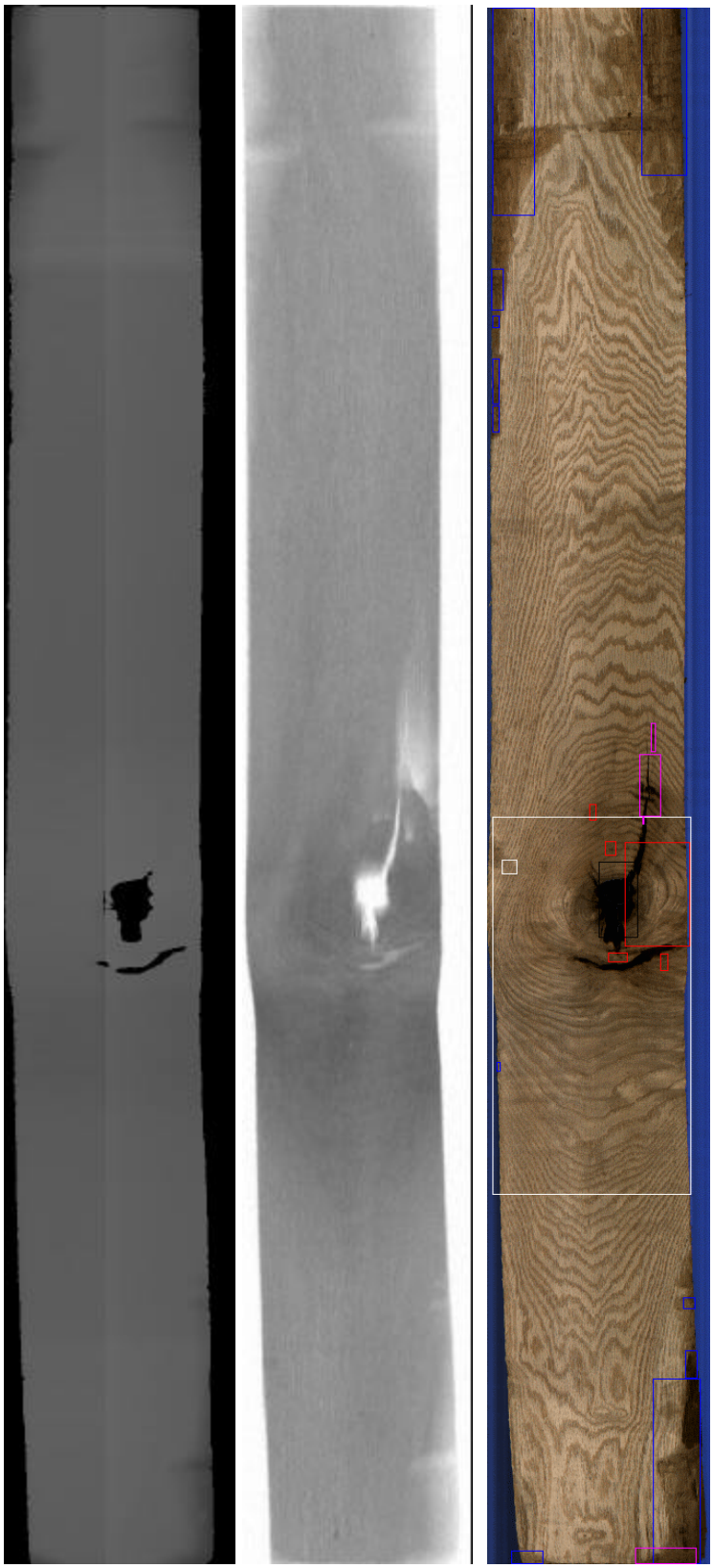

(a) (b) (c)

Figure 9.3 Wane at both end of the board were identified

light to be detected by the laser profiling hardware. Black areas like this in the laser image are assigned the "unknown class" during segmentation (see Chapter 6).

After the analysis of the laser image is completed the analysis of the X-ray image is begun. During the analysis of the X-ray image several defects are located and identified. These include the obvious hole that is in the center of the knot. This defect is marked with an admittedly hard to see black rectangle. Several knot areas were found. These are marked with red rectangles. Two high-density areas were found. These are marked with white rectangles. Note that one of these lies inside the other. In this machine vision system high-density and low-density areas will not be merged with any defect during the post-identification processing since high- and low-density areas are not visible on the board's surface. Finally, one large split area was found. The area is marked with the biggest pink rectangle shown in Figure 9.3 (c). This rectangle is located just above the large white rectangle.

All of these defects are, in fact, caused by one very large knot -- a big complicated defect -- in the middle part of the board. Since this knot consists of a complex mix of a large hole, splits and some tension wood, the analysis of the X-ray breaks the knot region up into a number of components and classifies each of these to produce multiple defects. Overall, this region is correctly identified as a defect area that would have to be removed during the crosscut operation.

During the analysis of the color image, several small areas of wane are located and identified. The areas that are identified as wane are marked with blue rectangles. These rectangles are all of the smaller ones and not the larger ones found during the processing of the laser image. These small wane areas are hard to detect during the analysis of laser image where only thickness information was used. However, they are located and correctly identified when information from all the three imaging modalities are used. It should be noted that some parts of wane areas that have almost the same thickness as the rest of the board, but they are slightly darker than clear wood. Two splits were also found. These areas are marked with small pink rectangles that lie around the larger split region identified in the X-ray processing. They also include a misidentified rather large split area found at the bottom of the board. This misclassification is caused, in part, by a small slice of the wane area that was not removed by the

operations discussed in Section 8.1, and, in part, by the image registration error that caused the color image to have one or two extra lines of dark pixels at the end of the board. This problem would be automatically corrected if the registration accuracy were improved.

An analysis of these examples together with other examples indicates that the module used to analyze the laser image can, in general, locate and correctly label wane and thin board defects since both of these defects have smaller range values than the correct value. Typically misclassifications occur 1) when a long thin board area is on the edge of the board and it is misclassified as wane; and/or 2) when a wane area crosses the entire width of the board and the area is misclassified as thin board. Since both of these defects, i.e., wane or thin board, must be removed during the crosscutting operation, it is not important that an accurate differentiation of these two classes be made. If a more accurate differentiation between these two classes were required, the efforts for improvement should focus on providing a better laser image with significantly improved dynamic range resolution.

The next set of examples is going to illustrate some of the characteristics of the X-ray image processing that is performed by the system. These examples will include only boards that contain neither wane nor too thin areas. Hence, the processing of the laser image provides no information regarding any defects that might be present. Given this situation the laser images for these examples will not be included in the figures.

The first of these examples is given in Figure 9.4. The top part of the board contains a large knot with a hole inside it. The hole was caused by part of the knot falling out at some time. The large knot (a dark area) and the hole (a rather bright area) are clearly visible in the X-ray image (Figure 9.4 (a)). The hole is correctly identified and marked by a black rectangle (see Figure 9.4 (b)). The wood around the hole is still part of the knot and has a high density as evidenced by it being darker than clear wood. Therefore, this area is identified as a knot. The hole and the knot area are not merged, as they normally would be. Both are shown in Figure 9.4 (b). Another large knot appears near the bottom of the board. This is also located and accurately identified. It is marked with the large red rectangle that appears in Figure 9.4 (b). As can easily

(a) (b)

Figure 9.4 A board contains knots and a hole

be seen, this knot has a fragmented structure that contains both a split-defect and a knot-defect. However, even in this case the vision system is able to detect all of the major parts, to merge these parts together, and, finally, to identify the combination as a knot. In fact, this fragmented structure can also provide richer information to further define fundamental wood defects. For example, any knot that includes a hole or a split is commonly referred to as an "unsound" knot, meaning that the knot is structurally unsound. A very small part of the knot, which is not detected during the analysis of the X-ray image, is located and identified later as a knot during the analysis of the color image. This area marked by a small red rectangle on the right side of the big rectangle. In this vision system no merging operation is performed to combine defects that have been assigned the same label but are located and identified by the different processing systems. Therefore, the above two parts of the big knot are not merged. Future research is needed to develop an efficient method that can merge these defects, and to use morphological information about individual defect fragments to more precisely classify a feature (e.g. an unsound knot vs. a sound knot).

The second of the examples to be considered is given in Figure 9.5. This example also contains knots and a high-density area. These knots and the high-density area are clearly visible in the X-ray image (Figure 9.5 (a)). The big knot area at the bottom of the board actually contains a knot and some tension wood, i.e., rather high-density wood that appears darker than clear wood in the X-ray image. Therefore, the module that processes the X-ray image recognized the whole area as a knot and marked it with a red rectangle (Figure 9.5 (b)). The full extent of such a high-density region is not truly a knot. However, since tension wood typically is very difficult, if not impossible, to machine an accurate differentiation of these two defect types is really not required for the crosscut application. Further research would be needed to add such abnormal wood structures as defects and to determine what unique measures could be used to distinguish them from knots.

Two knots, one in the middle of the board and the other just above the big knot area as just described, are also clearly visible in the X-ray image. The knots were located and correctly identified. This identification resulted in them being marked with red rectangles. An area located in the middle of the board is identified as a high-density area. This area is marked with a

(a) The X-ray image (b) The color image

Figure 9.5 A board that contains knots and wood of high-density

white rectangle. Clearly, the density of this area is higher (darker) than clear wood, as can be seen in Figure 9.5 (a). Although this area contains two small knots, the majority of this area has a color that is very close to clear wood. Therefore, this area is identified as a high-density area. Before the processing of the color image is begun, this area is removed from consideration as was discussed in Section 8.1. As a consequence, the two small knots are not detected during the analysis of the color image. During the analysis of the color image, only one smaller knot was located and identified. This very small knot is located in the lower half of the board. It is just visible in both the X-ray and color images but was located and identified correctly during the analysis of the color image.

These and other board examples that were processed suggest that the module used to process the X-ray image is generally capable of locating and identifying defects such as knots, holes, mineral streaks, splits, and high- and low-density components. This system will have misclassifications 1) when the knots or mineral streaks are too shallow, i.e., when a component of one of these defect types has a transmission value that is almost the same as clear wood; 2) when a knot area is long and narrow, i.e., when this area resembles mineral streak; and/or 3) when an area of mineral streak is very short and basically round, i.e., when this area resembles a knot. With regard to the first case, such defects will usually be located and identified during the analysis of the color image. As regard to the second case, since both of these defects are considered to be removable defects, little research was done to address this type of labeling error. If any of the above types of labeling errors cannot be tolerated then more research will have to be done on ways to improve the labeling accuracy. This research will probably involve the use of additional, more complex component measures.

The purpose of the next examples to be considered is to demonstrate in some detail the capabilities of the module that processes the color image. The first of these examples is shown in Figure 9.6. Like the other examples that were discussed above Figure 9.6 (a) shows the X-ray image of the board and Figure 9.6 (c) shows the color image of the board with the with the minimum-inscribing rectangle (MIR) of each defect overlaid on this color image. However, unlike the other examples Figure 9.6 (b) shows the connect component $BW_C(i, j)$ that is

generated during the low-level processing of the color image. The nature of this image will be described below.

The goal is to show that this module is capable of locating and identifying the defects that were not detected during the analysis of either the laser image or the X-ray image. This board contains many small knots, two high-density areas and several wane areas (see Figure 9.6 (c)). The results of the laser image processing included the location and identification of a large wane area at the top part of the board. This area is marked with a blue rectangle. The processing also found an area of thin board at the bottom of the image, which was misidentified as thin board. It, too, is marked with a blue rectangle. Note that this mislabeling is the result of an artifact that sometimes occurs in the laser image, i.e., a few lines at the end of an image have incorrect laser profile values.

During the analysis of the X-ray image, the two high-density areas (one at the top part, and the other at the bottom part of the board) are located and correctly identified. These areas are marked with white rectangles. Also, the larger knots are also located and identified during this analysis. These areas are marked with red rectangles. Before the analysis of the color image is begun all defect areas are removed from consideration (see Section 8.1). In fact, all pixels within the MIR of a defect component are removed from further consideration. These minimum-inscribing rectangles are shown the connected-component image, $BW_C(i, j)$ (Figure 9.6 (b)). All of these MIRs are green in color.

The remaining defects are detected and identified during the analysis of the color image. The results of the low- and intermediate-level processing of the color image are shown in Figure 9.6 (b). This figure shows the small knots, wane and other defect areas that were located. These areas are the ones that have various shades of pink.

During the high-level processing of color image, various small knots are correctly identified. These knots are marked with red rectangles in Figure 9.6 (c). . Some wane regions are identified as defect wane, e.g., wane at the up right corner of Figure 9.6 (c). Note that these small knots and wane defects in Figure 9.6 (c) do not correspond to any of the green rectangles

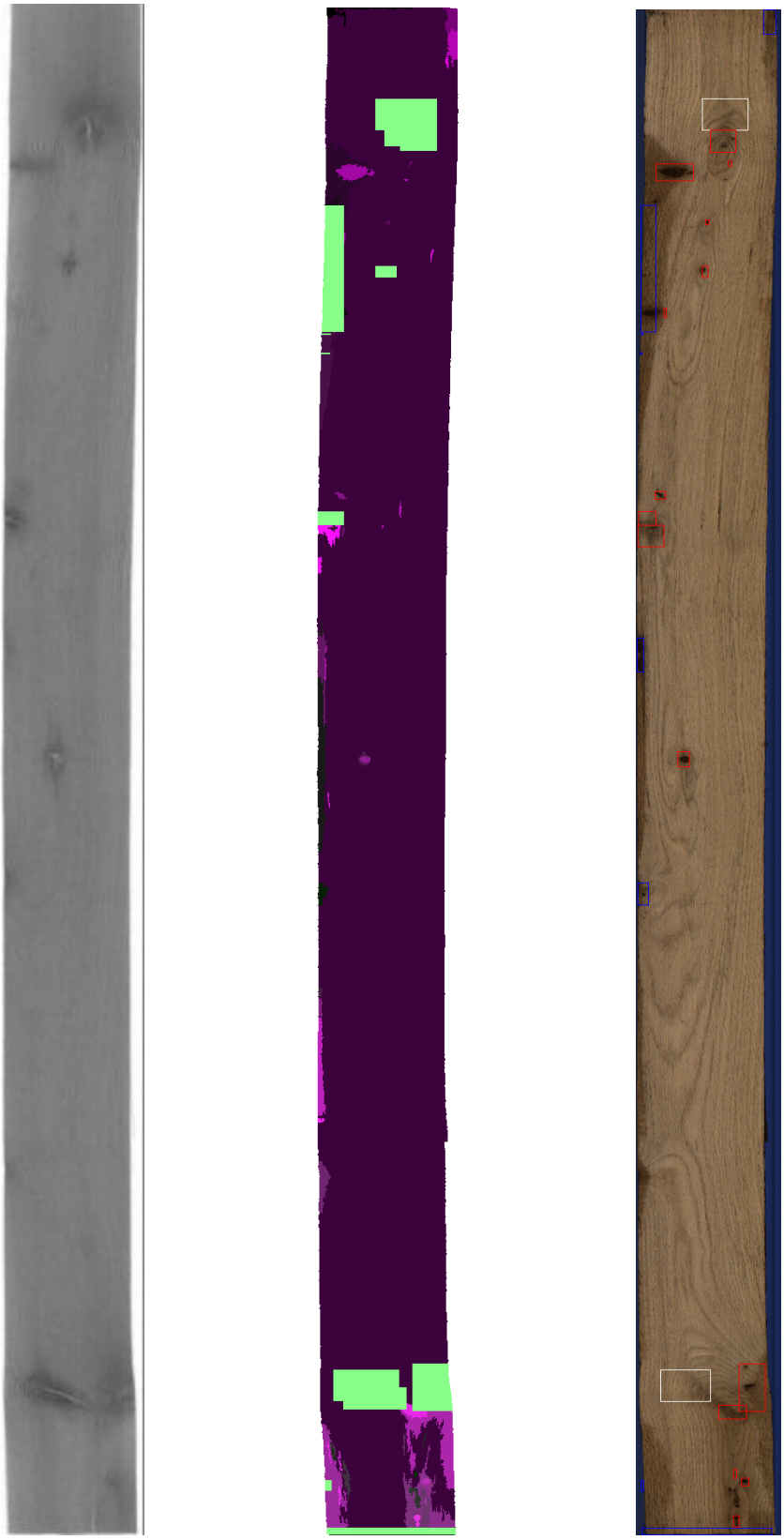

(a) The X-ray image (b) Connected-component image (c) The color image
Figure 9.6 Small knots and wane are detected during the analysis of the color image

in Figure 9.6 (b), but only to the connected component regions shown at various levels of pink. Also note that some of the defect areas shown in the connected-component image, do not receive any defect classification (i.e. they were classified as clear wood). For example, the wane areas at the bottom right-hand corner of the board have the almost correct thickness and are identified as clear wood even though their areas are quite large, i.e., these areas were not removed by any small area elimination process.

The second of this series of examples is shown in Figure 9.7. Here Figure 9.7 (a) is the color image of the board with the MIR for each defect that was identified overlaid upon it. Figure 9.7 (b) is again the connected component image, $BW_C(i, j)$. As before the areas that are pink are the components that have been found during the color image analysis. The green areas of Figure 9.7 (b) mark the MIR's of defects that have previously been identified, i.e., identified in either the processing of the laser image or the X-ray image.

Clearly, the two large knots have been identified before the analysis of color image begins. The many small areas of wane in the middle part of the board in Figure 9.7 (a) were located and correctly identified in the analysis of the color image. These areas are marked with blue rectangles. These wane regions were not detected during analysis of the laser image because their thickness is too close to correct board thickness. Two small knots (near the two large knots) are also detected during the analysis of the color images.

In summary the color vision module of this vision system can generally locate and identify surface knots, shallow mineral streak, and small splits/checks with reasonably good accuracy. However, it works much less accurate for the areas of shallow wane and areas of crayon mark. To accurately find and label these areas more research is needed. The specifications for this vision system allowed that shallow wane could be ignored or treated as clear wood if the thickness is very close to the correct thickness. As for crayon mark, there were not many samples of this available at the time this research was conducted and, hence, no effort was extended to identify such areas.

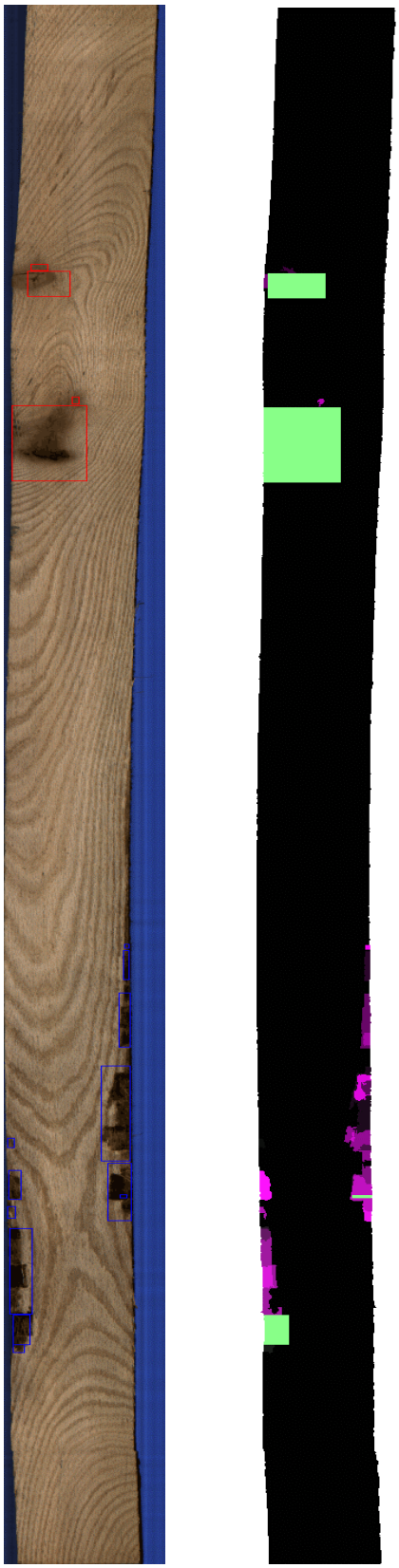

(a) (b)

Figure 9.7 Small areas of wane are identified

9.2 Independent Performance Validation

Kline and Surak [KLI00] performed a separate, completely independent, study to evaluate the performance of an automated hardwood lumber grading system. This system used this machine vision system to locate and identify the defects. A separate grading program used this information as input. The complete automatic lumber grading system was comprised of these two programs. Note, lumber grading is very labor intensive, is demanding, and is prone to errors. Consequently, there is every reason to want to automate this task. This section discusses the accuracy of this automatic lumber system that resulted from incorporating this machine vision system in its design.

9.2.1 Methods and Materials

To test this system, 89 red oak lumber boards were collected from various mills in the Appalachian region. These boards were true test samples in that they were different from the samples used to develop and train the machine vision system. The lumber was kiln-dried to within 5-8 percent moisture content. All boards were at least 2.1 m long and between 12 and 19 cm wide. The boards were surfaced with an abrasive planer to remove any surface roughness, stain, or soil marks, and to create a uniform thickness of 2.5 cm. This study considers 5 grades defined by the National Hardwood Lumber Association [NHL98]: First and Seconds (FAS), FAS 1-face (F1F), #1 Common (1C), #2 Common (2C), and #3A Common (3A). The grade mix consisted of 12, 8, 23, 20, and 26 boards of these NHLA grades, respectively, for a total of 89 boards. The boards were assigned a grade by a mill grader.

To test the accuracy of the automatic lumber grading system, the following hardwood lumber grade evaluations were conducted:

1. Automated Grade - the board sample was run through the lumber scanning system to generate laser, x-ray, and color images for each board face. These images were saved for subsequent processing and analysis. Subsequent processing utilized the computer vision software described in the earlier chapters to automatically generate a “digital map” of lumber grading defects in a standard format that could be used by

grading software. Hardwood lumber grading software, UGRS (Ultimate Grading and Remanufacturing System), was then used to grade each board based on the generated digital map [MOO98].

2. Digitized Grade - The boards were manually digitized for all grading defects. Digitization was done by hand and consists of mapping out and classifying all of the defects on the board according to the technique described by [AND93]. UGRS was then used to establish the true grade of the lumber based on the defects identified during manual digitization. Digitized grades are considered to be "ground truth" for evaluating the accuracy of automated grading.
3. NHLA Grade - the boards were graded by a NHLA employed certified professional grader to establish the market grade and value of the lumber.
4. Line Grade - the original grade of the boards as graded by the line graders at the various mills from which the board samples were collected.

Comparisons were then made between each of these grade evaluations to develop conclusions about the performance of the automated hardwood lumber grading system and where the system could be improved, i.e., where the machine vision system could be improved.

9.2.2 Results and Discussion

Table 9.1 shows the board-by-board grading accuracy of the Automated Grad compared to the actual or Digitized Grade. The Automated Grade correctly grades 56 boards, or 63 percent of the 89 boards studied. Note that this board-by-board comparison is a very strict evaluation of lumber grading accuracy and that while the accuracy of 63 percent may appear low, it compares favorably with the Line Grade, which correctly grades only 43 boards, or 48 percent of the boards (see Table 9.2).

Another assessment technique used was to determine the lumber value resulting from the different grading methods. Table 9.3 shows the value of the 89-board sample based on each of the grade evaluation methods. These values are based on the May 9, 2000 Hardwood Market

Table 9.1. Confusion matrix of board-by-board grading accuracy for the automatic lumber grading system. The most critical classification error can be seen in the #2 Common grade. The automated grader erroneously downgrades 9 boards as #2, where 7 should have been graded #1 and 2 should have been graded FAS/1-Face and better (From KLI03).

		Automated Grader					
		FAS/F1F	1	2	3A	3B or Below	Totals
Digitized	FAS/F1F	9	3	2			14
	1	1	5	7			13
	2	1	1	19	3	1	25
	3A		1	7	15	1	24
	3B or Below			1	4	8	13
	Totals:	11	10	36	22	10	89

Table 9.2. Confusion matrix for the Line grader. The most critical classification error can be seen in the #3B or Below grade. The line grader erroneously upgrades 11 boards as #3A and 2 as #2 (from KLI03).

		Line Grade					
		FAS/F1F	1	2	3A	3B or Below	Totals
Digitized	FAS/F1F	12	2				14
	1	5	7	1			13
	2	2	10	11	2		25
	3A	1	4	6	13		24
	3B or Below			2	11	0	13
	Totals:	20	23	20	26	0	89

Table 9.3. Value of the 89 boards for each of the grade evaluation methods in [HAR00] (from KLI03).

Evaluation Method	Value
Line Grade	$310
NHLA Certified Grade	$259
Digitized Grade	$247
Automated Grade	$244

Report [HAR00]. The Line Grade results in the highest value (the most optimistic value) of $310 for the sample. This value is 20 % higher than that estimated by the NHLA certified grade, i.e., NHLA Grade. The NHLA certified grade is commonly used to settle disputes in lumber grading. In terms of lumber value, the Automated Grade is closer to the NHLA Grade than the Line Grade. The Automated Grade gives the lowest lumber value (most conservative value) of $244. While the values between the NHLA and Automatic Grade were within 6% from each

other, this difference is greater than the 4 % money value allowance that is required by the NHLA grading specification. Even the difference between the NHLA and Digitized Grade methods is slightly greater than this 4% allowance at 4.6%.

There are many factors that can limit automatic grading accuracy. First, defining the "ground truth" or true grade of a board is a subjective process. For example, 8 sample boards were re-assigned a different grade by the same NHLA inspector during two separate NHLA grading sessions. Second, the are some aspects of the grading rules that lack precise definitions in UGRS. Examples, of these include surface measure rounding and clear cutting units. The lack of precise definitions of surface measure and clear cutting units can in some cases lead to a significant amount of rounding error that would cause errors in board grading. Third, there are some grading defects that the vision system must be able to identify for the grading application but it was not trained to do so because these wood features are not important in the crosscut application. Examples of these include sidebend [KLI00] and planer burn. In the case of planer burn, since the machine vision system was not trained to recognize this feature it usually classifies the simple surface discoloration as a knot, which is a critical grading defect. Finally, the results were adversely affected by some of the errors the vision system commonly makes. Perhaps the most significant of these is the vision system's habit of labeling roundish shaped mineral streak areas as being knots. Mineral streak is not typically considered a lumber grading defect but knots are. Note that in the crosscut application both mineral streak and knots are typically considered removable defects. Even given these limitations, the Automated Grade method generates a grading result that is more consistent with the Digitized Grade or "ground truth".

These results suggest that the vision system performed rather well for this application, given the fact that it was not trained to recognize everything that needs to be for the grading application and that some of the tolerable errors it makes, which have little impact on the crosscutting application can have a serious impact on the grading application.

A final conclusion that can be drawn from these results is that precise quantitative definitions of what constitutes a grading defect in lumber, which is currently qualitative in

nature, are needed before the true accuracy of automated lumber grading can be precisely assessed. Nevertheless, the defect recognition system presented in this research provides for the first time some of the tools that could be used to represent such qualitative judgments in numeric terms.

9.3 Summary

Examples presented here demonstrate that this vision system is capable of detecting and correctly identifying most of the major defects in hardwood lumber. This demonstration indicates that each of the four modules (preprocessing, analysis of laser image, analysis of X-ray image and analysis of color image) achieved the goals set forth in Chapter 1. Moreover, the low-level processing, the intermediate-level processing, and the high-level processing of all three imaging modalities can seemingly be utilized to perform useful tasks in the wood products industry.

The independent evaluation of the automatic lumber grading system performed by Kline and Surak [KLI03] also confirmed the performance of this vision system. In fact, the automatic lumber grading system was observed to be 31 percent more accurate than a typical lumber grader who establishes the grade and value of lumber at forest products industry plants. It is important to note that the system performed very well considering that the vision system was developed with a very limited number of samples. It also should be noted that the vision system was developed with images of sub-optimum quality since the development was done in parallel to the development of the image scanning hardware.

Chapter 10

Conclusions and Recommendation for Future Research

In the forest products secondary manufacturing industry, reduced availability high-grade hardwood lumber resources and recent marked price increases for high-grade lumber have forced manufacturers to make their products from lower-grade hardwood lumber. The use of lower grade lumber means that it takes more labor to produce rough parts. At the same time, the cost of the labor to convert lumber into rough parts has gone up, and there is a reduced availability of skilled people needed to do this conversion. These changes in raw material cost and labor cost are making it difficult for manufacturers to remain profitable. To survive in this increasingly complex and competitive environment, the industry is turning to machine vision systems to automate the conversion from lower-grade hardwood lumber to rough parts.

Researchers from government, universities, and industry have recognized the need for automating the conversion from lumber to rough parts in the forest products industry for a number of years. Clearly, an automatic sawing system that can remove defects in lumber while creating maximum yield would provide the solution to the above mentioned industrial problem [CON96, KLI96, CON97]. The major difficulty in creating an automatic sawing system is developing a machine vision system that can detect critical defects in wood that affect the quality of the rough parts produced. The challenge in creating such a machine vision system comes from the heterogeneous nature of hardwood lumber and from the image processing speed that is required to inspect the lumber at industrial production rates.

Given the complexity of inspecting hardwood lumber, researchers are increasingly turning to multiple sensors machine vision systems to locate and identify defects [CON92, AST92, HAG93, KLI96]. Of all the sensing modalities that have been studied by researchers, the following three sensing modalities seem to be the most appropriate for use in a multiple sensor vision system [CON92, KLI93, CON95]: 1) A color camera to detect surface features; 2) A laser range profiler to identify shape related defects; and 3) An X-ray scanner to locate internal

defects. However, little work has been done on designing and creating a machine vision system that combines all these sensing modalities.

The research work reported in this dissertation is the first aimed at creating a machine vision system that uses all of these imaging modalities. Note that while researchers have realized that color cameras [CON85, BRU90], laser range profiling systems [CON95] and X-ray scanners [CON95] are needed to inspect hardwood lumber, there have been no machine vision systems reported yet in literature that utilized all three of the above imaging modalities. Most vision systems that have been reported use either a single imaging sensor, typically a back and white camera [CON83, CHA89, CHO91] or an X-ray scanner [CON95], or two of the three image modalities mentioned above [HAG93, KLI93].

The goal of this research was to demonstrate the proof of concept for combining all these imaging modalities to show that not only can these modalities be used to detect most of the major defects but they can also be used to identify these major defects while the system operates at industrial speeds. This research was conducted at a time when computer speeds were on the order of about 200 megahertz, thus the emphasis on having the system operate at industrial speeds. The research project was aimed at a particular application, the real-time inspection of red oak lineals for the crossing cutting operation. This application was selected because it is thought to be the most challenging of all the inspection problems involving hardwood. Clearly, red oak is the most complex of the hardwoods to inspect and the cross cutting application involves locating and identifying the all the major defect types [CON97]. The result of this research work was included in U.S patent 5,960,104.

It should be pointed out that this research was conducted in parallel with the hardware development that was going on at Virginia Tech. The image collecting hardware for both the laser-profiling subsystem and the X-ray scanner was being developed in parallel with this vision software development. The hardware development team had spent a considerable amount of time and effort to continuously improve the quality of laser image and to combine the outputs of the two cameras on the profiling subsystem to form a range image. As a consequence, only a limited number of laser images were available for vision system development and the quality of

these images was not very good. As for the X-ray scanner, the voltage and current used to create the x-ray images could markedly affect the image quality. Consequently, the hardware team had to improve the contrast of the X-ray images and to maintain the stability of the imaging hardware. Also, some of the image collecting hardware was developed for use with IBM computers that had the Micro-channel bus. Later the decision was made to use computers that had the PCI bus. This meant that the hardware team had to redesign this collection hardware to run on PCI bus rather than the Micro-channel. Consequently, fully registered color images, laser images and X-ray images were at first not available at all. As the hardware development advanced, only a small number of images of hardwood lumbers became available to this research, but the image quality (especially, the image contrast) of laser range images and the X-ray images varied a good deal. All this means that this research was conducted in no small way in a data starved manner. This meant that certain data intensive methods of analysis could not be used in this vision system. Rather other approaches, ones that required far less data had to be used. Obviously, this impacted the directions this research could take.

All the algorithms used were implemented with the C programming language under the IBM OS/2 operating system. The software system has since been ported to Microsoft Windows NT. The only exceptions were the pre-processing algorithms. These were first implemented in C to verify their operation and then were programmed into the FPGAs on the MORRPH board. This computer vision system contains over 50 thousand lines of code.

The initial results obtained from this vision system demonstrate the feasibility of locating and identifying all the major defects that occur in hardwood lumber. This was even true during the initial hardware development phase when only images of unsatisfactory quality from a limited number of lumber samples were available to be processed. The vision system also has the capability to locate and identify these defects at the typical production speed of two linear feet per second. As was stated above, the vision system software was running on a relative slow computer (200 MHz Pentium processor) with aid from special image processing hardware that did all of the preprocessing operations, i.e., the MORRPH board.

A number of algorithms and methodologies were developed specifically for use in this vision system, algorithms and methodologies that might be useful in other applications as well. These include:

- A methodology is used that reduces the amount of data that needs to be processed by ordering the way in which the images from the different sensing modalities are analyzed. When multiple imaging sensors are used, each sensor increases the volume of data that must be analyzed. Given the processing speed requirements of two linear feet per second of hardwood secondary manufactures, the real-time detailed analysis of the data and the fusing of the information from all sensors can pose problems for any automatic inspection system. In the application considered in this research, the analysis of laser image is rather straightforward, and is performed first. Once areas with insufficient thickness are found, they are removed from consideration in the subsequent analysis of the X-ray and the color images. Removing these insufficient thickness defect areas from consideration in the analysis of the X-ray image not only improves the accuracy of locating and identifying defects but also reduces the amount of time needed to analyze the X-ray image. Similarly, defect areas such as knot and mineral streak found in the analysis of X-ray are removed from further consideration in the analysis of the color image. Just as is the case in the analysis of the X-ray image, removing these areas from consideration in the analysis of the color image improves both the accuracy of locating and identifying defects as well as reducing the amount of time needed to do the processing. The color imaging system produces three times the amount of data that is produced by either the laser imaging system or X-ray imaging system. Therefore removing defect areas from consideration in the color image analysis usually markedly reduces processing time of this image.

- A fuzzy logic algorithm is used to do defect labeling. The fuzzy logic approach, i.e., the approaching degree method [WAN83, ROS95], is used to mimic human behavior in identifying defects in hardwood lumber. Fuzzy logic approaches have found wide applications in process control and system control [RAS97]. However, little research work has been reported on applying fuzzy techniques to lumber inspection. The fuzzy

approaching degree method has been developed to identify defects in red oak lumber. Please note that one of the initial motivations for using this approach was the very limited number of images that were available when this research was begun. This limitation precluded using tradition pattern recognition methods and markedly limited the number of labeling approaches that could be considered. One benefit that has been noted by using this fuzzy approach is that the system seemingly does not make ridiculous errors as sometimes happens when more traditional pattern recognition approaches are used in decision making, i.e., when prototypical samples are misclassified.

- A connected component labeling algorithm is used that can handle non-binary segmented images. The segmentation method used in this vision system must be able to have multiple thresholds since at least three different kinds of pixels exist in the images from each of the imaging modalities. That is, pixels from any of these imaging modalities are either from clear wood, a defect area, or the background. Consequently, connected component labeling algorithms for binary images cannot be used on these images. This new algorithm is a computationally efficient method for handling non-binary images.

- A methodology is used for increasing the ability of the vision system to locate smaller defects by removing the effects of large defects from X-ray and color images. The X-ray image is analyzed first to locate and identified large defects such as mineral streak, big holes, and big knots. These large defects found are then removed from consideration and the X-ray image is analyzed again to detect small defects such as splits/checks and small holes. Please note that if small defects need not be detected or identified, the vision system can be easily reconfigured to detect only the larger defects. In the analysis of the color image, an analysis that is aimed primarily at detecting and identifying small defects, the large defects found in the analysis of the X-ray image are removed from consideration before the analysis of the color image is begun.

- An algorithm is used for reducing the amount of data that needs to be processed while preserving the system's ability to locate small cracks and other small surface defects. An image filter, the crack-preserving filter, has been developed that reduces the amount of

image data fed into the vision system while preserving the system's ability to detect small cracks and other fine defects.

As was stated above, this vision system can locate and identify most of the major defects that appear on a board's face or internally. However, as with most vision systems that work on real world applications, it makes errors particularly on small defects. As of this writing the impact of these errors on the cross cut application rough part yield is unknown. Please note that everyone agrees that sawyers make errors in cross cutting lineals. Some of these errors involve the lack of optimizing the cuts to increase part yield but other errors involve not removing all the defects that should have been removed from a part. Consequently, it is not well understood as of this writing exactly how the performance of the vision system and an optimized cutup program would compare with a sawyer. Collecting such information would provide insight into what areas of the vision system's performance are most critical to cross cut application.

Given this uncertainty here are the author's general views on ways the overall accuracy for locating and identifying defects can be improved:

Improve the fuzzy membership functions. The fuzzy membership functions described in this dissertation were created based on a very limited number of samples that were available to at the time this research was conducted. While every effort was made to optimize the performance of each defect recognition module, addition effort should put forth to validate and fine tune these fuzzy membership functions. This should involve the consideration of additional hardwood lumber samples and images taken with different contrasts or intensities.

Optimize the component measures to be extracted in the intermediate-level processing. Measure selection is an important step in building model-based vision systems. The selection of an optimal set of component measures should improve the performance of the high-level vision module. The major difficulty is in determining which set of measures will give good discrimination among the various defect classes while still being relatively easy (not very time-consuming) to compute. Further research on the selection

of an optimal of measures should improve vision system performance (both defect recognition speed and accuracy). Moreover, with the continued increase in computer speed and memory size, more computationally complex measures could be used in the near future while still maintaining the industrial throughput requirement of two linear feet per second.

Optimize program parameter that control low-level and intermediate-level processing. This computer vision system contains more than 50 thousand lines of code. The program uses numerous variables, variables that were described in Chapters 5 through 8, to control both the low and intermediate-level processing. At the time that this research was conducted there were only a very limited number of board images available upon which the values of these variables could be inferred. Their values, in reality, only represent the best estimates that could be made from a very limited database. It is believed that the performance of the system could be improved, perhaps markedly so, by creating a larger database of images so that better estimates of these parameter values could be made.

Refine the algorithms for the region merging. Defect regions such as knots, wane, and stains are oftentimes over fragmented. Knots, for example, can contain several splits. Parts of an area of wane can have the same thickness as clear wood. As a consequence, a defect such as a knot is often made up of several components that are not necessarily adjacent to each other. For the example given above they are not adjacent because split components lie between the components of knot. To handle such cases, a knowledge-based region merging method needs to be developed. Such a method should be able to eliminate the components that are small splits and merge the components that all belong to the same knot defect.

Adapting the vision system to different species of wood. While this vision system has been applied to other species of wood, namely, maple and pine, with some success, to refine its performance so that it can accurately handle these species requires additional research. Some of the defects that occur in maple or pine have different characteristics than these same defects in red oak. This means that the measures used to analyze these

and other species may have to be different from those used in the analysis of red oak. This also means that different defect recognition modules will have to be developed or that the current recognition modules might have to be revised. Finally, it should be noted that secondary manufacturing facilities typically only process one species of lumber at a time. Hence, when the species is changed the version of the vision system used could also be changed so that it is maximized for the species that is to be processed.

Improving the software implementation. As mentioned before, the vision system software was first developed under IBM OS/2, and then was ported to Microsoft Windows NT 4.0. This was done under a very tight time schedule. Since this system contains over 50 thousand lines of code it is highly probable that given all the porting that it has experienced the structure of this program could undergo a restructuring that could improve its readability, its maintainability, and perhaps even its operating speed.

As was stated above the vision system is not 100 percent accurate in either its ability to detect or identify defects. However, neither are the humans that perform the various inspection tasks that are performed in the forest products industry. The real question then is whether this system can perform a task as well as a human inspector even given the errors that it currently makes. Unfortunately, for the application for which the system was designed there have been no studies done to determine how well this system, working as a front end for an automatic cross cut program, would perform in relation to the human sawyer. But there has been a study, one that was mentioned in Chapter 9 of this dissertation, that does provide some guidance about this system's performance on another application, the grading of hardwood lumber. In the United States the hardwood lumber grading process is controlled by the National Hardwood Lumber Association (NHLA). This association is responsible for the defining the rules that are used in the grading process and are also responsible for resolving any grading disputes that arise between a buyer and a seller. When this vision system was used as the front end for an automatic lumber grading program, this combination was able to out perform skilled NHLA certified lumber graders by 31 percent. This fact has two implications. First it clearly indicates that a machine vision system need not be perfect in order to be of utility to the forest products industry. This is

obviously a very important point. And secondly it implies that perhaps this system would allow an automatic cross cut system to favorably compare with a yield of a human sawyer.

References

[ABD93] Abdulghafour, M and M. A. Abidi, "Data fusion through non-deterministic approaches -- a comparison", Proceeding of SPIE, Vol. 2059, Boston, 1993.

[AGG77] Aggarwal, J. K., et al., "Computer methods in image analysis", Los Angeles: IEEE Computer Society, 1977.

[AND93] Anderson, R. B., R. E. Thomas, C. J. Gatchel, and N. D. Bennett, "Computerized technique for recording board defect data". Res. Pap. NE-671. Radnor, PA: U.S. Department of Agriculture, Forest Service, Northeastern Forest Experiment Station, 1993.

[ARG90] Argialas, Demetre, "Computational image interpretation models: an overview and perspective", Photogrammetric Engineering and Remote Sensing, vol. 56, no. 6, pp. 871-886.

[AST92] Astrand, E., "Detection and classification of surface defects in wood: A preliminary study". Dept. of Electrical Engineering, Linkoping University, LiTH-ISY-I-1437, 1992.

[AUN89] Aune, Jan E., et al., "Lumber Optimizer", United States Patent No. 4,879,752, 1989.

[AUN91] Aune, Jan E., and K. L. Peter, "Log Scanner", United States Patent No. 5,023,805, 1991

[BAL82] Ballard, D. H., and C. M. Brown, *Computer Vision*, Englewood Cliffs, New Jersey: Prentice-Hall, Inc., 1982.

[BAR88] Bartlett, S., C. Cole, and R. Jain, "Automatic solder joint inspection," IEEE Transactions on Pattern Analysis and Machine Intelligence, vol. 10, no 1, pp. 31-44, Jan. 1988.

[BAT93] Batchelor, B. G., "Automated inspection of bread and loaves", Proceedings of SPIE, vol. 2064, pp. 124-134, 1993.

[BAT97] Batchelor, Bruce G. and Paul F. Whelan, *Intelligent Vision System for Industry*, Springer-Verlag, 1997.

[BAY93] Bayro-Corrochano, Eduardo, "Review of automated visual inspection 1983-1993", part I and part II, SPIE vol. 2055, Intelligence Robots and Computer Vision XII, 1993.

[BEC91] Bechtold, W. A. and R. M. Sheffield. "Hardwood timber supplies in the United States", Tappi Journal, vol. 74, no.5, pp. 111-116, 1991.

[BEN90] Benhabib, B., C. R. Charette, K. C. Smith and A. M. Yip, "Automatic visual inspection of printed circuit boards". International Journal of Robotics and Automation, vol. 5, no. 2, pp. 49-58, 1990.

[BER91] Berger, Ulrrich, et al., "Automatic inspection of manufactured parts in the one-of-a-kind production", Proceedings of SPIE, vol. 1615, pp. 124-134, 1991.

[BHA95] Bhanu, Bir, Sungkee Lee, and John Ming, "Adaptive image segmentation using a genetic algorithm", IEEE Trans. on Systems, Man, and Cybernetics, vol. 25, no. 12, pp. 1543-1561, 1995.

[BLO96] Bloch, I., "Information combination operators for data fusion: A comparative review with classification", IEEE Trans. on Systems, Man, and Cybernetics, Part A: Systems and Humans, vol. 26, no. 1, pp. 52-67, 1996.

[BOG87] Bogler, P. L., "Shafer-Dempster reasoning with applications to multi-sensor target identification systems", IEEE Trans. on SMC, vol. 17, no. 6, 1987.

[BRI96] Brink, A.D., "Using spatial information as an aid to maximum entropy image threshold selection", Pattern Recognition Letters, pp. 29-36, 1996.

[BRO92] Brown, Lisa G., "A survey of image registration techniques", ACM Computing Surveys, vol. 24, no. 4, pp. 325-376, 1992.

[BRU90] Brunner, C. C., et al., "Using color in machine vision systems for wood processing", Wood and Fiber Science, vol. 22, no. 4, pp. 413-428, 1990.

[BRZ93] Brzakovic, D., H. Beck, and P. Shanmugham, "Defect characterization and classification for web materials", Proceedings of IEEE International Conference on Speech and Signal Processing, Minneapolis, MN, pp. 44-47, 1993

[BUS90] Bush, R. J., S. A. Sinclair, and P. A. Araman. "Matching your hardwood lumber to current market needs", Southern Lumberman, vol. 25, no. 7, pp. 24-27, 1990.

[CHA89] Chang, S. J., J. R. Olson, and P. C. Wang, "NMR imaging of internal features in wood". Forest Products Journal, vol. 39, no. 6, pp. 43-49, 1989.

[CHE88] S. S., Chen, "Adaptive control of multisensor systems", Proceedings of SPIE, Vol. 931, Orlando, April 1988.

[CHI88] Chin, R. T., "SURVEY: automated visual inspection: 1981 to 1987", Computer Vision, Graphics, and Image Processing, vol. 41, pp. 346-381, 1988.

[CHO90a] Cho, T-H, R. W. Conners and P. Araman, "A computer vision system for automatic lumber detection using blackboard expert system method", Proceedings of 10th International Conference on Pattern Recognition, Atlantic City, NJ, June, 1990.

[CHO90b] Cho, T-H, R. W. Conners, and P. A. Araman. "A computer vision system for automated grading of rough hardwood lumber using a knowledge-based approach", Proceedings of IEEE Systems, Man and Cybernetics Society, Los Angeles, CA, pp. 345-350, November, 1990.

[CHO90c] Cho, T-H, et al., "A computer vision system for analyzing images of rough hardwood lumber", Proceedings of 10th Int'l Conf. on Pattern Recognition, vol.1, pp. 726-728, 1990.

[CHO91] Cho, T-H, "A knowledge-based machine vision system for automated industrial web inspection", Ph.D. Dissertation, Virginia Polytechnic Institute and State University, Blacksburg, Virginia, 1991.

[CHO93] Chou, P. B., et al., "Automatic defect classification for integrated circuits", Proceedings of SPIE, vol. 1907, pp. 95-103, 1993.

[CHU93] Chu, C. and J. K. Aggarwal, "The Integration of image segmentation maps using region and edge information", IEEE trans. Pattern Anal. Mach. Intelligence, vol. 15, no. 12, Dec., 1993.

[CIC92] Ciccotelli, J. and J. F. Portala, "Applications of artificial vision in the wood industry", Industrial Metrology, no.2, pp. 185-194, 1992.

[CLO71] Clowes, M., "On seeing things", Artificial Intelligence, vol.2, no.1, pp.79-112, 1971.

[COH82] Cohen P. R. and E.A. Feigenbaum, *The Handbook of Artificial Intelligence*, Addison-Wesley, Vol. III, 1982.

[CON83] Conners, R.W., et al., "Identifying and locating surface defects in wood: part of an automated lumber processing system", IEEE Trans. on PAMI, vol. 5, no. 6, pp. 573-583, 1983.

[CON85] Conners, R.W., et al., "Utility of color information in the location and identification of defects in surfaced hardwood lumber", First International Conference on Scanning Technology in Sawmilling, 1985.

[CON87] Conners, R.W., "The need for a quantitative model of human pre-attentive vision", Proceedings of SPIE, vol. 786, Application of Artificial Intelligence, pp. 211-220, 1987.

[CON89] Conners, R.W., et al., "A system for identifying defects in hardwood lumber that uses AI methods", IEEE Proc. 231 Sourth-east Coast Conf., 9-12, April, Columbia, SC, vol. 3, pp. 1080-1084, 1989.

[CON95] Conners, R.W., D. E. Kline, and P.A. Araman. "Developing a multi-sensor scanning system for hardwood inspection and processing". Proceedings, 2nd International Workshop on Scanning Technology and Image Processing on Wood, Skelleftea, Sweeden, pp. 107-118, 1995.

[CON97] Conners, R.W., D. E. Kline, P. A. Araman, and T. H. Drayer, "Machine vision technology for the forest products industry", IEEE Computers, vol.30, no.7, pp. 43-48, 1997.

[COX94] Cox, Earl, *The Fuzzy Systems Handbook*, Academic Press, Inc., 1994.

[DAR88] Darwish, A. M. and A. K. Jain, "A rule based approach for visual pattern inspection", IEEE Trans. on PAMI, vol. 6, no.5, pp. 555-577, 1988.

[DAV92] Davies, E. R., *Machine Vision: Theory, Algorithms, Practicalities*. Academic Press, 1992.

[DRA95] Drayer, T. H., et al., "A modular reprogramming real-time processing hardware, MORRPH", Proc. Symp. Field Programmable Gate Arrays '95, IEEE Press, Piscataway, NJ, 1995.

[DRA96] Drayer, T. H., "A design methodology for creating programmable logic-based real-time image processing hardware", Ph.D. Dissertation, Virginia Tech, 1996.

[DUD73] Duda, R. and P. Hart, *Pattern Classification and Scene Analysis*, New York: John Wiley, 1973.

[DUR87] Durrant-Whyte, H. F., "Consistent integration and propagation of disparate sensor obervations", Intl. J. of Robotics Research, vol. 6, no. 3, 1987.

[EJI89] Ejiri, M., et al., "Knowledge-directed inspection for complex multilayered patterns", Machine Vision and Applications, vol. 2, no. 3, pp. 155-166, 1989.

[FAU86] Faugeras, O. D., et al., "Building visual maps by combining noisy stereo measurements", Proceedings of IEEE International Conference on Robotics and Automatic Systems. San Francisco, CA, 1986.

[FLO89] Floyd, S. L., and S. L. Washburn, "Method for Determination of Pith Location Relative to Lumber Surfaces", United States Patent No. 4,831,545, 1989.

[FOR95] Discussions with Mr. William Fortney of Aristokraft, Inc., 1995.

[FOR96] Personal communications with Mr. William Fortney of Aristokraft, Inc., 1996.

[FOR97] Forslund, Donald C., "Advanced Manufacturing Inspection System", United States Patent No. 5,659,630, 1997.

[FU81] Fu, K. S., and J. K. Mui, "A survey of image segmentation", Pattern Recognition, vol. 13, no. 1, pp. 3-16, 1981.

[FUN85] Funt B. B., and E. C. Byant, "A computer vision system that analyzes CT-scans of sawlogs", Proceedings of IEEE Conference on Computer Vision and Pattern Recognition, pp. 175-177, 1985.

[GAR81] Garvey, T. D., J. D., Lowrance, and M. A. Fischler, "An inference technique for integrating knowledge from disparate sources", Proceedings of 7th Int. Joint Conf. Artifical Intellegence, pp. 319-325, 1981.

[GIL83] Gil, Baldemar, et al., "Experiments in combining intensity and range edge maps", Computer Vision, Graphics, and Image Processing, vol. 21, pp. 395-411, 1983.

[GON92] Gonzalez, R. C., and R. E. Wood, *Digital Image Processing*, Addison-Wesley Publishing Company, 1992.

[GUO92] Discussions with Guo, Lichun of Spatial Data Analysis Laboratory at Virginia Tech, 1992.

[HAB93] Haberstroh, Richard and Ivan Kadar, "Multi-spectral data fusion using neural networks", Proceedings of SPIE: Signal Processing, Sensor Fusion, and Target Recognition II, vol. 1955, pp. 65-75, 1993.

[HAG93] Hagman, P. O., and S. Grundberg, "Multivariate image analysis methods to classify features on Scots Pine: evaluation of a multi-sensor approach". 5th International Conference on Scanning Technology and Process Control for the Wood Products Industry, Atlanta, GA, October 25-27, 1993.

[HAN88] Hanson, A. R., et al., "Sensor and information fusion from knowledge-based constraints", Proceedings of SPIE, vol. 931, Orlando, 1988.

[HAN93] HAN, Joon H. Doo M. Yoon and Myeong K. Kang, "Features for automatic surface inspection", Proceedings of SPIE, Vol. 1907, pp. 114-123, 1993.

[HAR00] Hardwood Market Report Lumber News Letter, vol. 78, no. 19. Hardwood Market Report, Memphis, Tennessee, 2000.

[HAR84] Haralick, R.M., "Digital step edges from zero crossing of second directional derivatives". IEEE Transactions on Pattern Analysis and Machine Intelligence, vol.6, no.1, pp. 58-68, 1984.

[HAR85] Haralick R.M., and L.G. Shapiro, "Survey images segmentation techniques", IEEE Trans. on CVGIP 29, pp. 100-132, 1985.

[HAR88] Hara, Y., H. Doi, K. Karasaki and T. Iida, "A system for PCB automated inspection using fluorescent light", IEEE Transactions on Pattern Analysis and Machine Intelligence, vol.10, no. 1, pp. 69-78, 1988.

[HAR92] Haralick R. M., and L. G. Shapiro, *Computer and Robot Vision*, Volume 1, Addison-Wesley, 1992.

[HAT89] Hatje, Giinter H., "Method and System for Optically Testing Sawn Timber for Faults", United States Patent No. 4,827,142, 1989.

[HEN88] Henderson, T. C., "Multisensor knowledge systems", Proceedings of SPIE, Vol. 931, Orlando, 1988.

[HUB85] Huber, H. A., C.W. McMillin and J.P. McKinney. "Lumber defect detection abilities of furniture rough mill employees", Forest Product J. vol. 35, pp. 79-82, 1985.

[HUB92] Huber H. A., and T. J. Manetsch, "An economic and system analysis of the automated lumber processing system (ALPS)". Forest Prod. J., vol. 42, pp. 51-56, 1992.

[HOU93] Hou, Y. J., "Developing a flexible range sensing system for industrial inspection applications", Master Thesis, Virginia Tech, 1993.

[JAI89] Jain, A. K., *Fundamentals of Digital Image Processing*, Englewood Cliffs, New Jersey: Prentice Hall, 1989.

[JAI89a] Jain, Ramesh, et al., "Machine vision for semiconductor wafer inspection", Machine Vision for Inspection and Measurement, Academic Press, 1989.

[JAI95] Jain, Ramesh, Rangachar Kasturi and Brian G. Schunck. *Machine Vision* McGraw Hill, 1995.

[JAK88] Jakubowicz, O. G., "Autonomous reconfiguration of sensor systems using neural nets", Proceedings of SPIE, Vol. 931, Orlando, 1988.

[KAM85] Kamat, S. J., "Value function structure for multiple sensor integration", Proceedings of SPIE, Vol. 579, Cambridge, 1985.

[KAN82] Kandel, Abraham, *Fuzzy Techniques in Pattern Recognition*, John Wiley and Sons, 1982.

[KAS86] Kashyap, R. L., "Image models", *Handbook of Pattern Recognition and Image Processing*, New York: Academic Press, 1986.

[KAU75] Kaufmann, A., *Introduction to the Theory of Fuzzy Subsets*, Volume I, Academic Press, 1975.

[KEN90] Kenway, D. J., "A supercomputer-based machine vision grading system and trimmer optimizer for dimension lumber", Proceedings of the Process Control/Production Management of Wood Products: Technology for the '90s, Athens, Georgia, 1990.

[KLI03] Kline, D. E., C. Surak, and P. A. Araman. "Automated hardwood lumber grading utilizing a multiple sensor machine vision technology", Computers and Electronics in Agriculture, vol. 41, pp. 139-155, 2003.

[KLI93] Kline, D. E., R. W. Conners, D. L. Schmoldt, P. A. Araman, and R. L. Brisbin, "Multiple sensor machine vision system for automatic hardwood feature detection". The 5th International Conference on Scanning Technology & Process Control for the Wood Industry, Atlanta, Georgia, 1993.

[KLI97] Kline, D. E., et al., "Scanning hardwood lumber for processing and grading - what to do now and why", The 7th International Conference on Scanning Technology & Process Optimization for the Wood Product Industry, pp. 49-59, 1997.

[KOC96] Koczy, L. T., "Fuzzy if … then rule models and their transformation into one other", IEEE Transactions on Systems, Man, and Cybernetics, Part A: Systems and Humans, vol. 26, no. 5., 1996.

[LAC97] Discussions with Paul Lasasse of Spatial Data Analysis Laboratory at Virginia Tech, 1997.

[LON94] Longest, H. Cary, et al, "High speed, high resolution web inspection system". United States Patent No. 5,305,392, 1994.

[LOU88] Lou, R. C., and M. Lin, "Robot multi-sensor fusion and integration: optimum estimation of fused sensor data", Proceedings of IEEE International Conference on Robotics and Automation, April 1988.

[LOU92] Lou, C. and M. G. Kay, *Data Fusion in Robotics and Machine Intelligence*, Academic Press, 1992.

[LOU93] Loughlin, C., *Sensors for Industrial Inspection*, Kluwer Academic Publichers, 1993.

[LUP91] Luppold, W. G. "Hardwood lumber demand in the 1990's", Proceedings of the 19th Annual Hardwood Symposium of the Hardwood Research Council. Starkeville, Mississippi, pp. 57-63, 1991.

[LUP93] Luppold, W. G., "Decade of change in the hardwood industry", Proceedings of the Twenty-first Annual Hardwood Symposium of the Hardwood Research Council, pp. 11-24, 1993.

[LUP94] Luppold, W. G., "Are perceived shortages of hardwood lumber real?" The Northern Logger & Timber Processor, vol. 43, pp. 12-14, 1994.

[LUP95] Luppold W. G., and J. E. Baumgras. "Price trends and relationships for Red Oak and Yellow-Poplar stumpage, sawlogs, and lumber in Ohio: 1975-1993", Northern Journal of Applied Forestry, vol. 12, no. 4, pp. 168-173, 1995.

[LUR94] Luria, Marc, Maty Moran, and Dan Yaffe, "DCS-1: A fuzzy logic expert system for automatic defect classification of semiconductor wafer defects", Proceeding of IEEE, 1994.

[MAR80] Marr, D., and E. Hildreth, "Theory of edge detection", Proceedings of the Royal Society of London (Series B), vol. 200, pp. 269-294, 1980.

[MAR87] Martin, R. P., P. Collet, P. Barthelemy, and G. Roussy. "Evaluation of wood characteristics: internal scanning of the material by microwaves". Wood Science Technology, vol. 21, pp. 361-371, 1987.

[MAT86] Matthews, P. C. and J.F. Soest, "Method for determining localized fiber angle in a three dimensional fibrous material", United States Patent No. 4,606,645, 1986.

[MCD80] McDonald, K. A., "Lumber defect detection by ultrasonics". Research Paper FPL-311. Madison, Wisconsin: U. S. Department of Agriculture, Forest Service, Forest Products Lab, 1980.

[MCK85] Mckeown, D. M., et al, "Ruled-based interpretation of aerial images", IEEE Transactions on Pattern Analysis and Machine Intelligence, vol. 7, no. 5, pp. 570-585, 1985.

[MIL87] Miller, W. T., "Sensor-based control of robotic manipulators using a general algorithm", IEEE J. of Robotics and Automation, vol. 3, no. 2, 1987.

[MIL90] Miller, J. S., and Jesse C. Arnold, *Introduction to Probability and Statistics*, 2nd edition, McGraw Hill, 1990.

[MIT86] Mitiche, Amar and J. K., Aggarwal, "Multiple sensor integration/fusion through image processing: a review", Optical Engineering, vol. 25, no. 3, pp. 380-386, 1986.

[MOO95] Moore, Stuart G., "Optical scanning device for lumber", United States Patent No. 5,412,220, 1995.

[MOO98] Moody, John, Charles J. Gatchell, Elizabeth S. Walker, and Powsiri Klinkhachorn. "User's guide to UGRS: the Ultimate Grading and Remanufacturing System (version 5.0)". USDA Forest Service General Technical Report, GTR-NE-254, 1998.

[MOR94] Morris J. and J. Notarangelo, "Machine vision for metal inspection", Proceedings of SPIE, vol. 2183, pp. 130-136, 1994.

[MTU89] Ntuen, C. A., et al., "KIMS: a knowledge-based computer vision system for production line inspection", Computer Industrial Engineering, vol. 16, no. 4, pp. 491-508, 1989.

[MUR96] Murphy, P.R., "Biological and cognitive foundations of intelligent sensor fusion", IEEE Trans. on Systems, Man, and Cybernetics, Part A: Systems and Humans, vol. 26, no. 1, pp. 42-51, 1996.

[NAK89] Nakamura, Y. and Y. Xu, "Geometrical fusion method for multi-sensor robotic systems", Proceedings of IEEE Int. Conf. on Robotics, Automation and systems, Scottsdale, Arizina, 1989.

[NAZ84] Nazif, A. M., and M. D. Levine, "Low level image segmentation: an expert system", IEEE Transactions on Pattern Analysis and Machine Intelligence, vol. 6, No. 5, pp. 555-567, 1984.

[NEV86] Nevatia, R., "Image segmentation", *Handbook of Pattern Recognition*, Ed. T.Y. Young and K.S. Fun, Academic Press, pp. 215-245, 1986.

[NHL98] National Hardwood Lumber Association (NHLA). Rules for the Measurement and Inspection of Hardwood and Cypress. National Hardwood Lumber Association, Memphis, Tennessee, 1998.

[OHL78] Ohlander, Ron, et al., "Picture segmentation using a recursive region splitting method", IEEE Trans. on Computer Graphics and Image Processing, vol. 8, pp. 313-333, 1978.

[OHT80] Ohta, Yu-ichi, et al., "Color information for region segmentation", IEEE Trans. on Computer Graphics and Image Processing, vol. 13, pp. 222-241, 1980.

[PAU82] Pau, L. F., "Fusion of multi-sensor data in pattern recognition", *Pattern Recognition Theory and Applications*, D. Reidel Publishing Company, pp. 189-201, 1982.

[PAU83] Pau, L. F., "Integrated testing and algorithms for visual inspection of integrated circuits", IEEE Trans. on PAMI, vol.5, pp. 602-608, 1983.

[PAU88] Paul, D., et al., "VISTA: Visual interpretation system for technical applications - architecture and use", IEEE Transaction on Pattern Analysis and Machine Intelligence, vol. 10, no.3, 1988.

[PAU89] Pau, L. F., "Knowledge representation approaches in sensor fusion", Automatica, vol. 25, 1989.

[PAU90] Pau L. F., and X. Xiao, "Knowledge-based sensor fusion editor", IEEE Trans. on Systems, Man, and Cybernetics, vol. 26, no. 1, pp. 42-51, 1990.

[PAV77] Pavlidis, T., *Structural Pattern Recognition*, Springer-Verlag, 1997.

[PIE91] Pietikainen, M., et al., "The design of advanced vision systems for industrial inspection", Proceedings of SPIE, vol. 1615, pp. 172-178, 1991.

[POE95] Poelzleitner, Wolfgang, "Syntactic recognition of defects on wooden boards", Proceeding of SPIE Int. Soc. Opt. Eng., vol. 2588, 1995.

[POL94] Polzleitner, W. and A. Niel, "Automatic inspection of leather surface", Proceedings of SPIE, vol. 2347, pp. 50-58, 1994.

[POP94] Popovic, D. and N. Liang, "Fuzzy approach in model-based object recognition, Proceedings of 3rd IEEE Intl. Conf. in Fuzzy Systems, Orlando, USA, pp. 1801-1808, June 1994.

[POR92] Portala, J. F., and J. Ciccotelli, "Nondestructive testing techniques applied to wood scanning", Industrial Metrology, vol. 2, pp. 299-307, 1992.

[POS92] Postaire, J. G. and M. Ameziane, "A pattern classification approach to multilevel thresholding for images segmentation", *Computer Vision and Image Processing*, Academic Press, 1992.

[PRA91] Pratt, W., *Digital Image Processing*, second edition, John Wiley & Sons, Inc., 1991.

[RAH97] Rahman, S. C. and E. R. Hkan, "Neural-Fuzzy logic control system with adjustable fuzzy logic membership functions", United States Patent No. 5,594,835, 1997.

[REG92] Regalado, C., D. E. Kline and P. Araman, "Optimum edging and trimming of hardwood limber", Forest Products Journal, vol. 42, no. 2, pp.8-14, Feb. 1992.

[ROB65] Roberts, L., "Machine perception of three-dimensional solids", Optical and Electro-Optical Information Processing, Ed. J. Tippet, et al., MIT Press, 1965.

[ROG89] Roggemann, Michael C., et al., "Multi-sensor information fusion for target detection and classification", Proceeding of SPIE, vol. 931, p8-13, 1989.

[ROS82] Rosenfeld, A. and A. C. Kak, *Digital Picture Processing*, 2ed. Academic Press, New York, 1982.

[ROS95] Ross, Timothy J., *Fuzzy Logic With Engineering Applications*, McGraw-Hill, Inc., 1995.

[ROW92] Rowa, P., "Automatic visual inspection and grading of lumber", Proceedings of Scanning Technology and Image Processing of Wood, August 30 - September 1, Skelleftea, Sweden, 1992.

[RUM89] Rummel, Peter, "Applied robot vision combining work-piece recognition and inspection", *Machine Vision for Inspection and Measurement*, Academic Press, pp. 203-221, 1989.

[SAH88] Sahoo, P. K., et al., "A survey of thresholding techniques", IEEE Trans. on Computer Graphics and Image Processing, vol. 44, pp. 233-260, 1988.

[SAN88] Sanz, J. L., and D. Petkovic, "Machine vision algorithms for automated inspection of thin-film disk heads", IEEE Trans. on PAMI, vol. 10, no. 6, pp. 830-848, 1988.

[SAW77] Sawchuk, A. A., "Real-time correction of intensity nonlinerarities in imaging system", IEEE Transaction on Computers, vol. 26, no.1, pp. 34-39, 1977.

[SEV78] Sevdlow, Martin, et al., "Image registration: similarity measure and preprocessing method comparisons", IEEE Trans. on Aerospace and Electronic Systems, vol. 14, no. 1, pp. 141-149, 1978.

[SHA76] Shafer, G., *A Mathematical Theory of Evidence*, Princeton University Press, 1976.

[SHI87] Shirai, Y., *Three-Dimensional Computer Vision*, Springer-Verlag, 1987.

[SMY88] Smyrniotis, C. and K. Dutta, "A knowledge-based system for recognizing man-made objects in aerial images", Proceedings of IEEE Conference on Computer Vision and Pattern Recognition, 1988.

[SZY81] Szymani, R. and K. A. McDonald, "Defect detection in lumber: state of the art", Forest Products Journal, vol. 31, no. 11, pp. 34-43, 1981.

[WAL86] Waltz, E. L. and D. M. Buede, "Data fusion and decision support for command control", IEEE Trans. on SMC, vol.16, no. 6, 1986.

[WAL90] Waltz, E. L. and J. Llinas, *Multisensor Data Fusion*, Artech House, 1990.

[WAN90] Wan, E.W., "Neural network classification: a Baesian interpretation", IEEE Trans. on Neural Network, vol. 1, no. 4, pp. 303-305, 1990.

[WAN92] Wang, L. X., "Fuzzy systems are universal approximators", Proceedings of IEEE International Conference on Fuzzy Systems, San Diego, CA, pp. 1163-1169, 1992.

[YOU86] Young, T.Y and K. S. Fu, *Handbook of Pattern Recognition and Image Processing*, Academic Press, 1986.

[YOU92] Young, K and S. Fu, *Handbook of Pattern Recognition and Image Processing*, Academic Press, 1992.

[ZAD73] Zadeh, L. A., "Outline of a new approach to the analysis of complex systems and decision processes", IEEE Transactions on Systems, Man, and Cybernetics, vol. 3, No. 1, 1973

[ZHA93] Zhang, G. and A. Wallace, "Physical modeling and combination of range and intensity edge data", IEEE Trans. on CVGIP:Image Understanding, vol. 58, no. 2, pp. 191-220.

[ZHU91] Zhu, D., et al., "CT image segmentation for defect region identification", Proceedings of SPIE, San Diego, July 1991.

[ZHU93] Zhu, D., A feasibility study on hardwood log inspection using CT imagery analysis, Ph.D. dissertation, Virginia Tech, 1993.

[ZIM87] Zimmerman, H.J., "Fuzzy sets", *Decision Making and Expert Systems*, Kluwer, Boston, 1987.

Vita

Xiangyu Xiao was born in November 1959, in Henan, China. He received a BS degree from the Department of Information and Control Engineering, Xi'an Jiaotong University, Xi'an, China, in 1982, and a MS degree in Electrical Engineering from Virginia Polytechnic Institute and State University, Blacksburg, Virginia, in 1993. In 2004, he received a Ph.D. degree in Electrical Engineering, also from Virginia Polytechnic Institute and State University.